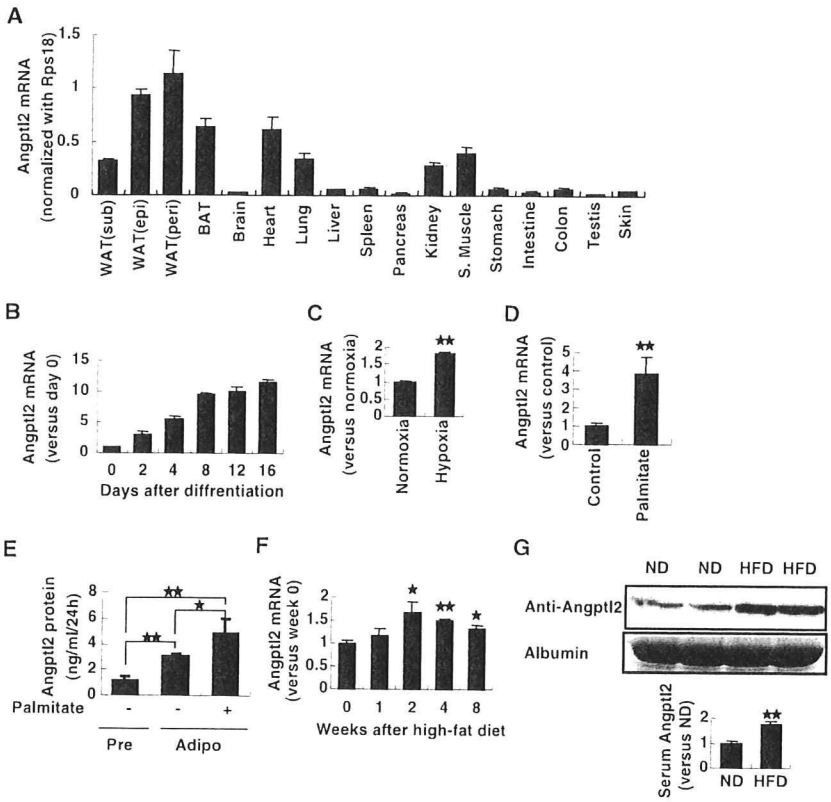

Figure 1. Angptl2 Is Secreted by Adipose Tissue

(A) Angptl2 mRNA expression in various tissues of mice fed normal chow (n = 4). WAT, white adipose tissue; sub, subcutaneous; peri, perirenal; mes, mesenteric; BAT, brown adipose tissue; S. Muscle, skeletal muscle.

(B–D) Angptl2 mRNA expression in 3T3-L1 cells during adipocyte differentiation (n = 3) (B), in differentiated 3T3-L1 cells incubated under hypoxic conditions (1% O_2, 24 hr, n = 3) (C), and in cells treated with palmitate (200 μM, 24 hr, n = 4) (D).

(E) Angptl2 protein levels in culture medium of pre- (Pre) or postdifferentiated (Adipo) 3T3-L1 cells with or without palmitate treatment (200 μM, 24 hr, n = 4).

(F) Angptl2 mRNA expression in the mesenteric adipose tissue of obese mice fed a high-fat diet for the indicated periods starting at 8 weeks of age (n = 4).

(G) Representative western blot and quantitative evaluation of serum Angptl2 protein in mice fed a normal diet (ND) or a high-fat diet (HFD) for a period of 8 weeks (n = 4). CBB-stained albumin is as control bands for protein loading. Data are the mean ± SEM, *p < 0.05 and **p < 0.01 compared with controls.

Fibrinogen-binding integrins are abundantly expressed by monocytes/macrophages and endothelial cells, and fibrinogen must undergo oligomerization or polymerization to display its activity. The presence of extravascular fibrinogen at sites of inflammation has been documented by pathologists for decades (Dvorak et al., 1985). These findings prompted us to ask whether an oligomeric protein derived from adipose tissue and containing a fibrinogen-like sequence might play a pathological role in inflammatory changes of adipose tissue associated with obesity. Recently, we and others identified seven angiopoietin-like proteins (Angptls), which possess a coiled-coil domain at the N terminus for oligomerization and a C-terminal fibrinogen-like domain (Kim et al., 1999; Kubota et al., 2005a; Oike et al., 2004). Angptls are structurally similar to Tie-2 receptor ligands (angiopoietins), but Angptls do not bind to either Tie2 or the homologous Tie1 protein, indicating that their role differs from that of angiopoietins.

Here we show that angiopoietin-like protein 2 (Angptl2) is primarily secreted by adipose tissue and that its expression is increased by obesity and obesity-related pathological conditions, including hypoxia and endoplasmic reticulum (ER) stress. We found that increased circulating Angptl2 levels were closely related to adiposity, systemic insulin resistance, and inflammation in both mice and humans. Angptl2 acted on endothelial cells and monocytes/macrophages via integrin signaling, resulting in the promotion of inflammation. Constitutive activation of Angptl2 in mouse skin tissue induced chronic inflammation, including inflammatory changes of the vasculature characterized by abundant attachment of leukocytes to the vessel walls and increased permeability. Deletion of Angptl2 led to reduced inflammation in adipose tissue and ameliorated systemic insulin resistance in mice with dietary obesity. Conversely, persistent overexpression of Angptl2 in adipose tissue caused local inflammation and systemic insulin resistance in nonobese mice. These findings establish Angptl2 as a key adipocyte-derived inflammatory mediator linking obesity to systemic insulin resistance and identify it as a new molecular target that could be used to improve the diagnosis and treatment of obesity and related metabolic diseases.

RESULTS

Angptl2 Expression in White Adipose Tissue Is Increased by Obesity and Obesity-Related Stress

Angptl2 mRNA was widely expressed in various organs of mice, but its level was particularly elevated in visceral white adipose tissues (Figure 1A). Differentiated 3T3-L1 adipocytes expressed Angptl2 mRNA (Figure 1B), and its expression was increased by hypoxia (Figure 1C), which occurs in obese adipose tissue (Hosogai et al., 2007; Nishimura et al., 2008; Schenk et al., 2008; Ye, 2009). We found significantly increased ER stress in adipocytes from obese mice compared with cells from nonobese mice (see Figure S1 available online). Serum levels of long-chain saturated fatty acids (LCSFAs) are elevated in obesity, and LCSFAs promote ER stress in adipocytes (Schenk et al., 2008). Our in vitro study of cultured 3T3-L1 cells revealed that ER stress was induced in adipocytes after treatment with palmitate, one of the LCSFA, or thapsigargin, an ER stress inducer. As

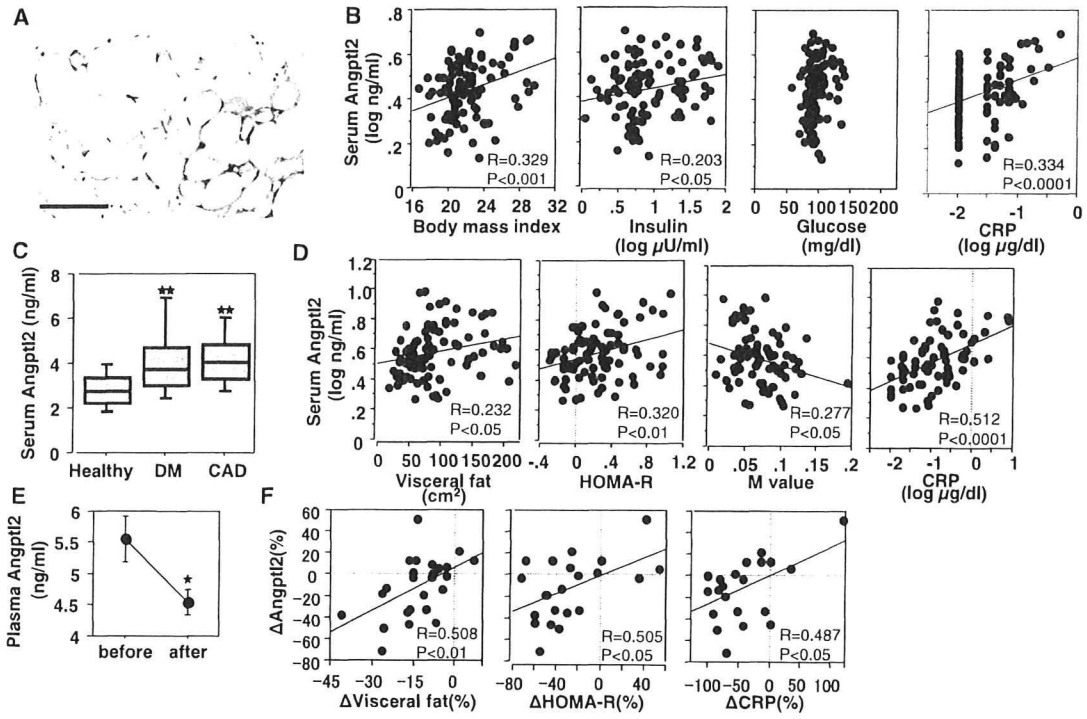

Figure 2. Circulating Angptl2 Is Correlated with Adiposity, Insulin Resistance, and Inflammation in Humans

(A) Immunohistochemical staining for Angptl2 in human adipose tissue. Scale bar, 100 μm.

(B) Correlation of the serum Angptl2 level with the body mass index or serum insulin, glucose, and CRP levels in healthy volunteers (n = 98).

(C) Serum Angptl2 levels in healthy volunteers (Healthy, n = 98) and in patients with type 2 diabetes (DM, n = 89) or coronary artery disease (CAD, n = 109). Horizontal bars represent the 10%–90% percentile range, and boxes indicate the 25%–75% percentile range. The horizontal line in each box corresponds to the median.

(D) Correlation of the serum Angptl2 level with the visceral fat area, HOMA-R index, M value, and CRP level in diabetic patients.

(E and F) Changes of the plasma Angptl2 level in obese diabetic male patients after pioglitazone treatment (n = 27). Plasma Angptl2 levels (mean ± SEM) before and after treatment (E). Correlation of the change (%) of the plasma Angptl2 level with the change (%) of the visceral fat area, subcutaneous fat area, HOMA-R index, and CRP level. Correlation coefficient (R) and probability (P) values are shown (F). *$p < 0.05$ and **$p < 0.01$ compared with controls.

a result, both the cellular Angptl2 mRNA level and its protein concentration in the culture medium were significantly increased (Figures 1D and 1E, Figure S2, and data not shown). Angptl2 mRNA in mesenteric white adipose tissue and serum Angptl2 protein levels were increased in obese mice fed a high-fat diet (Figures 1F and 1G), suggesting that Angptl2 is a bioactive adipocyte-derived factor that has a role in obesity and related metabolic diseases.

Circulating Angptl2 Level Is Correlated with Adiposity, Systemic Insulin Resistance, and Inflammation in Humans

Immunohistochemical analysis revealed that Angptl2 was expressed by the adipocytes of human adipose tissue (Figure 2A). We analyzed the circulating levels of Angptl2 in various human subjects by using an enzyme-linked immunosorbent assay (ELISA). In healthy normal-weight volunteers aged from 20 to 59 years, the serum Angptl2 concentration ranged from 1.36 to 4.98 ng/ml, and the distribution was normal after log transformation (Figure S3A). Plasma levels were comparable and strongly correlated with the corresponding serum levels (Figure S3B). There was no significant difference of serum Angptl2 concentration between genders (data not shown). Angptl2 level showed a positive correlation with body mass index, serum insulin level, and serum C-reactive protein (CRP) level. In contrast, the level of Angptl4, which has already been identified as an adipocyte-derived Angptl, showed no correlation with these factors in normal-weight healthy subjects (Figure 2B and Figure S4). An increase of the body mass index, serum insulin level, and CRP level is associated with the development of type 2 diabetes and atherosclerosis (Eckel et al., 2005; Mokdad et al., 2003). Indeed, serum Angptl2 was also significantly increased in patients with type 2 diabetes or coronary artery disease (Figure 2C). In 935 consecutive persons aged 27–84 years who underwent a medical checkup and gave informed consent for measurement of serum Angptl2 at the Japanese Red Cross Kumamoto Health Care Center, the Angptl2 level was positively correlated with the body mass index, abdominal circumference, and serum CRP level (Figure S5). In patients with type 2 diabetes, Angptl2 was positively correlated with the visceral fat area, homeostasis model assessment of insulin resistance (HOMA-R) index (Matthews et al., 1985), and serum CRP level, but not with the subcutaneous fat area. Angptl2 level was inversely correlated with the insulin sensitivity index (M value), as assessed

by the hyperinsulinemic euglycemic clamp test (DeFronzo et al., 1979) (Figure 2D).

These observations led us to ask whether improvement of systemic insulin resistance or inflammation would influence the circulating level of Angptl2. We observed a significant decrease of the plasma Angptl2 level in 27 obese diabetic men following treatment with pioglitazone at 30 mg/day for 3 months (Figure 2E). The percent decrease of the plasma Angptl2 level was correlated with the percent decrease of the visceral fat area, HOMA-R index, and serum CRP level (Figure 2F). These results suggested that visceral fat was likely to be the main source of circulating Angptl2, the concentration of which was significantly correlated with systemic insulin resistance and inflammation.

Angptl2 Activates Migration and Inflammatory Changes of Endothelial Cells and Monocytes/Macrophages via Integrins

Since the vasculature has an important role in tissue inflammation (Jackson et al., 1997), we examined the effect of Angptl2 on endothelial cells. First, we found a dose-dependent increase of cell adhesion when human umbilical vein endothelial cells (HUVECs) and human arterial endothelial cells (HAECs), which express several integrins on their surfaces, were plated on Angptl2-coated plates (Figures 3A and S6). We next analyzed cell adhesion in the presence of a series of function-blocking antibodies for specific integrins. A neutralizing antibody for integrin $\alpha5\beta1$ inhibited endothelial cell adhesion to Angptl2-coated plates, as did RGD peptide, which blocks RGD-dependent integrins (Figure 3B), suggesting that Angptl2-induced endothelial cell adhesion was an $\alpha5\beta1$-dependent process, although the involvement of untested integrins could not be excluded. Integrin $\alpha5\beta1$ activates NF-κB in endothelial cells (Klein et al., 2002). Consistently, there was increased translocation of NF-κB to the nucleus and degradation of IκB in HUVECs stimulated with recombinant human Angptl2 protein (Figures 3C and 3D).

Angptl2 also promoted the migration of HUVECs and HAECs through a microchemotaxis membrane (Figure 3E). Time-lapse imaging of HUVECs or HAECs cultures revealed that protrusion of lamellipodia and membrane ruffling were rapidly induced following the addition of Angptl2 (Movies S1 and S2). Since Rac1, a small Rho-GTPase, plays a pivotal role in the protrusion of lamellipodia, membrane ruffling, and cell migration (Bar-Sagi and Hall, 2000; Fryer and Field, 2005), we investigated whether Rac1 was activated in HAECs and HUVECs by performing a pull-down assay. Activation of Rac1 was detected in both Angptl2-stimulated HUVECs and HAECs (Figure 3F). In viable Angptl2-stimulated HUVECs, a single-molecule probe was used to determine Rac1 activity, showing that it was diffusely activated at the plasma membrane, with this activation being followed by protrusion of lamellipodia and membrane ruffling (Figure 3G and Movie S3). Moreover, Angptl2 no longer stimulated the protrusion of lamellipodia and membrane ruffling in HUVECs transfected with a dominant-negative Rac1 mutant expressing red fluorescent protein (RacN17-IRES-RFP) (Figure 3H and Movie S4). These findings suggest that Angptl2-stimulated lamellipodia formation and membrane ruffling in endothelial cells were both mediated by activation of Rac1. Next, we investigated whether Angptl2 could induce in vivo chemotaxis of endothelial cells in a mouse cornea assay. Implanted pellets containing Angptl2 markedly induced neovascularization in the mouse cornea, whereas pellets containing PBS alone did not (Figure 3I). Monocytes/macrophages express several integrin receptors that are responsible for adhesion, migration, and extravasation into the peripheral tissues (Friedl and Weigelin, 2008; Rose et al., 2007). We found that the THP-1 human monocytic cell line expressed integrins $\alpha4$, $\beta1$, $\beta2$, and $\alpha5\beta1$ (Figure 3J). THP-1 cells adhered to Angptl2-coated plates in a dose-dependent manner (Figure 3K). FACS analysis revealed that Angptl2 bound to THP-1; this binding was completely inhibited by neutralizing antibodies for integrins $\alpha4$ or $\beta2$ and was partially blocked by antibodies for integrin $\alpha5\beta1$ or $\beta1$ (Figure 3L). Angptl2 also promoted transmigration by THP-1 cells and primary human monocytes (Figure 3M and Figure S7).

Constitutive Angptl2 Activation Induces Local Inflammation in Mouse Skin Tissue

To further investigate the role of Angptl2 in the inflammatory process, we generated transgenic mice expressing Angptl2 driven by the keratinocyte-specific promoter K14 (K14-Angptl2) and therefore constitutively expressing Angptl2 in the epidermis (Figures S8A and S8B). The ears, snouts, and eyelids of K14-Angptl2 mice were redder than those of controls. The tails of K14-Angptl2 mice were not only reddish but also swollen and showed loss at the tips (Figure 4A), indicating local inflammation. Lectin staining showed an increase of adherent leukocytes, a common feature of inflammatory vasculature (McDonald, 1994), in enlarged vessels of the skin tissue specimens from K14-Angptl2 mice (Figure 4B), while there was no difference of vessel length between the genotypes (Figure S8C). The vessels of K14-Angptl2 mice were significantly more permeable than the vessels of wild-type controls after inflammation was induced by topical application of mustard oil, a potent proinflammatory agent (Figure 4C). As expected, even before mustard oil application, lumens of $CD31^+LYVE\text{-}1^+$ lymphatics were enlarged in the skin of K14-Angptl2 mice, while such changes were not observed in controls (Figure 4D), suggesting that increased drainage via lymphatics was compensating for the excessive leakiness of Angptl2-stimulated vessels in the dermis. These findings indicate that Angptl2 induces inflammatory vascular remodeling rather than angiogenesis.

Reduction of Adiposity and Obesity-Related Adipose Tissue Inflammation in *Angptl2*$^{-/-}$ Mice

Next, we investigated the pathophysiological role of Angptl2 by generating Angptl2 knockout (*Angptl2*$^{-/-}$) mice (Figure S9). *Angptl2*$^{-/-}$ mice were born alive following Mendelian inheritance and appeared to be grossly normal. Interestingly, when fed normal chow, *Angptl2*$^{-/-}$ mice weighed slightly less (Figure S10A) and had a lower body fat mass estimated by computed tomography (CT) (Figures S10B and S10C) than heterozygotes or wild-type mice fed the same normal diet, although there was no significant difference of daily food intake or energy expenditure between the groups (Figures S10D and S10E). In addition, *Angptl2*$^{-/-}$ mice showed slightly, but significant, better glucose tolerance and insulin sensitivity (Figures S10F and S10G). Next, we fed 8-week-old mice a high-fat diet containing 32% (wt/wt) fat to stimulate weight gain. After

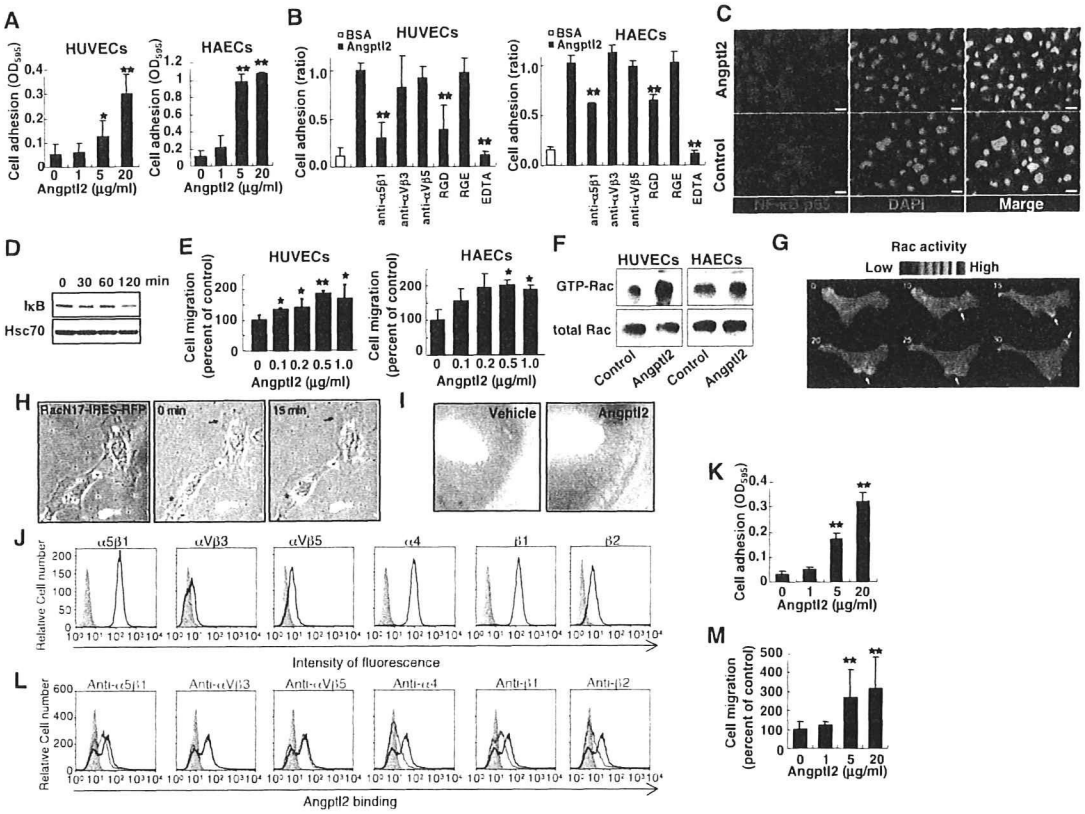

Figure 3. Angptl2 Activates Endothelial Cells and Monocytes

(A) Adhesion of HUVECs or HAECs to culture dishes coated with various concentrations of recombinant human Angptl2 (n = 3).

(B) HUVECs or HAECs were preincubated with or without 25 μg/ml of blocking antibodies (anti-α5β1, anti-αvβ3, or anti-αvβ5) or RGD or RGE peptides (300 μM), and cell adhesion was assessed (n = 3). As a negative control, cell adhesion was assayed in the presence of 10 μM EDTA, which inhibits integrin binding.

(C) Nuclear translocation of NF-κB subunit p65 in HUVECs at 2 hr after Angptl2 stimulation. Nuclei were counterstained with 4′,6′-diamidino-2-phenylindole (DAPI). Scale bar, 20 μm.

(D) Representative western blots of IκB and Hsc70 protein (internal control) in HUVECs at the indicated times after Angptl2 stimulation.

(E) Migration of HUVECs or HAECs in response to Angptl2 (n = 4).

(F) HUVECs or HAECs were cultured with Angptl2 for 30 min and then subjected to the pull-down assay using GST-PAK-CRIB followed by western blotting with anti-Rac1 antibody. Representative images are shown.

(G) HUVECs expressing Raichu-Rac1 (a probe for active Rac1) at the indicated times (min) after Angptl2 stimulation. Arrows indicate nascent and retracting lamellipodia. Ratio ranges are shown on the right.

(H) HUVECs that were either untransfected or transfected with RacN17 (shown in red in the left panel and by red stars in the center and right panels) and stimulated with Angptl2 at time 0 and 15 min. Angptl2-stimulated membrane ruffling is observed in HUVECs without RacN17 (arrows).

(I) Macroscopic appearance of neovascularization in the mouse cornea. Pellets containing vehicle or Angptl2 (0.5 μg) were implanted into micropockets cut in the corneal stroma.

(J) Integrin expression by THP-1 cells. Typical profiles obtained by FACS analysis with the indicated anti-integrin antibodies (black line traces) or isotype-matched control IgG (filled gray traces).

(K) Adhesion of THP-1 cells to culture dishes coated with various concentrations of Angptl2 (n = 3).

(L) Inhibition of Angptl2 binding to THP-1 cells by integrin-neutralizing antibodies. THP-1 cells were preincubated with (red line traces) or without (blue line traces) the indicated anti-integrin neutralizing antibodies, and then incubated with FLAG-tagged Angptl2 followed by detection with FITC-conjugated anti-FLAG antibody. Negative controls (filled gray traces) had omission of Angptl2.

(M) Migration of THP-1 cells in response to Angptl2 (n = 7–9). Data are the mean ± SD, *$p < 0.05$ and **$p < 0.01$ compared with controls.

8 weeks of high-fat diet feeding, *Angptl2*$^{-/-}$ mice had a body weight 12% lower than that of wild-type mice (Figure 5A). The visceral and subcutaneous fat mass and total body fat percentage were moderately decreased in *Angptl2*$^{-/-}$ mice compared to wild-type mice (Figures 5B and 5C). Considerable accumulation of fat was seen in the liver and skeletal muscle of wild-type mice, whereas these changes were mild in *Angptl2*$^{-/-}$ mice (Figures 5D and 5E). Although there were no obvious differences of food intake or energy expenditure between the two groups, the respiratory quotient was significantly lower in the *Angptl2*$^{-/-}$ group (Figures S11A–S11C).

We next examined the expression of mRNAs for inflammatory cytokines (IL-6 and TNF-α), a chemokine (MCP-1), various macrophage markers (F4/80, CD68, CCR2, Mgl1, and Mgl2),

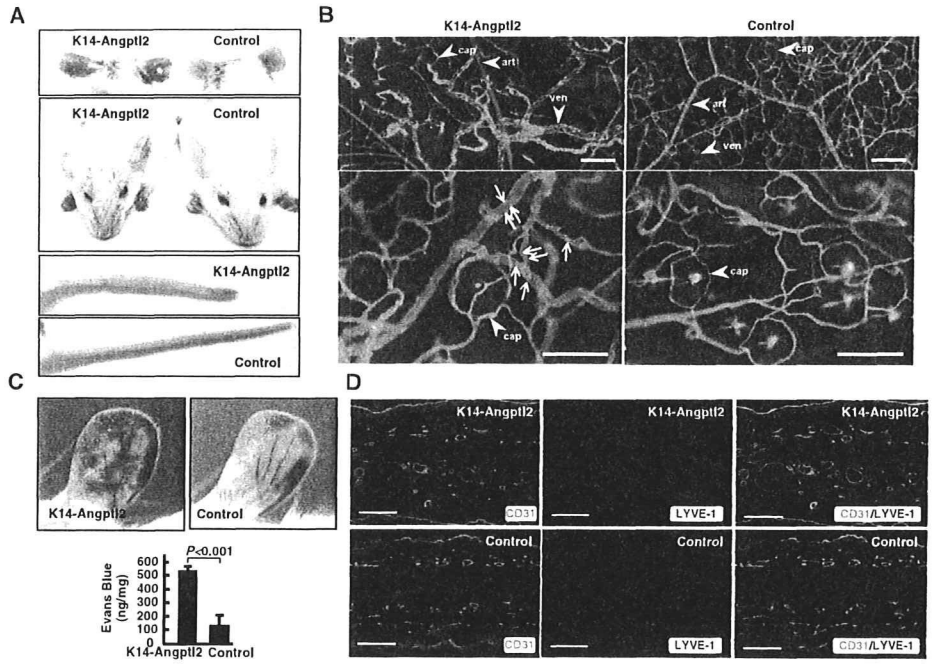

Figure 4. Sustained Angptl2 Overexpression Induces Vascular Inflammation

(A) Appearance of 6-month-old transgenic K14-Angptl2 and control mice.

(B) Ear skin blood vessels from transgenic and control mice. Arrows indicate adherent leukocytes on the walls of enlarged vessels from K14-Angptl2 mice. Arrowheads with art, ven, and cap in each panel indicate arteriole, venule, and capillary, respectively. Scale bar, 200 μm.

(C) Evans blue dye leakage into the skin of the ear following treatment with mustard oil as an inflammatory agent. Representative images and quantitative values are shown (mean ± SD, n = 7).

(D) Immunohistochemistry of ear skin from K14-Angptl2 and control mice with anti-CD31 and anti-LYVE-1 antibodies. Representative photographs are shown. Scale bar, 100 μm.

and insulin-sensitizing adipocytokines (adiponectin and leptin) in the adipose tissue of mice fed a high-fat diet. As shown in Figure 5F, adiponectin expression was increased, while TNF-α and general (F4/80, CD68) and inflammatory (CCR2) macrophage markers were all decreased in the adipose tissue of *Angptl2*$^{-/-}$ mice. However, the expression of residential macrophage markers (Mgl1 and Mgl2) remained unchanged. Furthermore, expression of F4/80 mRNA was positively correlated with the adipose tissue weight in controls, indicating that adiposity was significantly correlated with macrophage infiltration into adipose tissue. In contrast, there was no significant correlation between adipose tissue weight and macrophage infiltration in *Angptl2*$^{-/-}$ mice (Figure 5G), suggesting that this decrease of macrophage infiltration may be independent of reduced adiposity in *Angptl2*$^{-/-}$ mice. Furthermore, immunohistochemistry using the macrophage marker Mac2 revealed accumulation of Mac2-positive macrophages in crown-like structures within the adipose tissue of wild-type mice, while fewer Mac2-positive cells were observed in the adipose tissue of *Angptl2*$^{-/-}$ mice (Figure 5H). The high-fat diet caused impaired glucose tolerance and insulin resistance in controls, whereas *Angptl2*$^{-/-}$ mice showed better glucose tolerance and insulin sensitivity based on the results of intraperitoneal glucose and insulin tolerance tests (GTT and ITT, respectively) (Figures 5I and 5J). To explore which organ(s) contributed to the improved insulin sensitivity in *Angptl2*$^{-/-}$ mice, we next performed western blotting analysis of the insulin signaling pathway. Tyrosine phosphorylation of insulin receptor β and serine phosphorylation of Akt after insulin injection were significantly increased in both the liver and skeletal muscle of *Angptl2*$^{-/-}$ mice compared with wild-type mice (Figure 5K). To confirm these results, we performed hyperinsulinemic-euglycemic clamp experiments. Both glucose infusion rate and whole-body glucose disposal rate were significantly increased in *Angptl2*$^{-/-}$ mice, while clamp endogenous glucose production was significantly reduced. In addition, the percent decrease in endogenous glucose production from basal to clamp states was significantly higher in *Angptl2*$^{-/-}$ mice than in wild-type mice (Figure 5L). These results indicated that insulin sensitivity was improved in both the skeletal muscle and liver of *Angptl2*$^{-/-}$ mice fed a high-fat diet.

Angptl2 Promotes Local Inflammation in Adipose Tissue and Systemic Insulin Resistance

Finally, we determined whether sustained overexpression of Angptl2 in adipose tissue promoted systemic insulin resistance by generating transgenic mice that overexpressed Angptl2 in adipose tissue under the control of aP2, an adipose tissue-specific promoter (aP2-Angptl2) (Figure S12A). Based on the level of Angptl2 expression, we considered that line 5 was the most acceptable model for examining the pathological role of increased Angptl2 expression in obese mice (Figure S12B), so we performed subsequent analyses using line 5 and wild-type

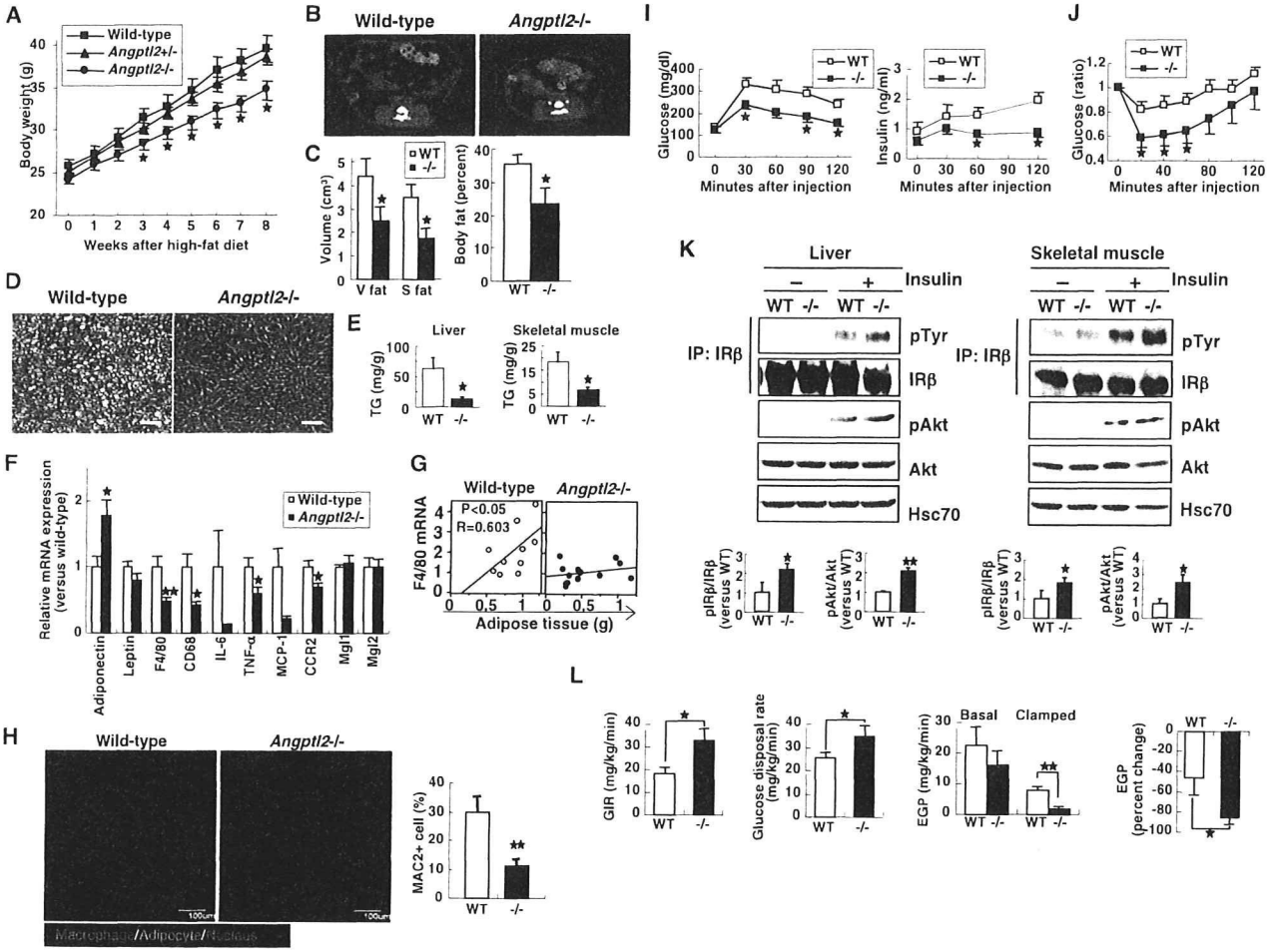

Figure 5. Deletion of Angptl2 Reduces Adipose Tissue Inflammation and Systemic Insulin Resistance in Dietary Obese Mice

Analyses of *Angptl2*$^{-/-}$ and wild-type mice fed a HFD for 8 weeks (A–L).

(A) Body weight of each genotype (n = 8–16 per group) at the indicated times (weeks) after initiation of a HFD.

(B and C) Representative CT findings (B) and quantitative comparison of the visceral (V) and subcutaneous (S) fat volume and total percent body fat (C) in *Angptl2*$^{-/-}$ mice and wild-type mice (n = 5–7 per group).

(D) HE-stained liver sections from *Angptl2*$^{-/-}$ and wild-type mice. Scale bar, 100 μm.

(E) Triglyceride (TG) content of liver and skeletal muscle from *Angptl2*$^{-/-}$ mice and wild-type mice (n = 6 per group).

(F) Quantitative RT-PCR of mRNAs encoding adipocytokines and macrophage markers in epididymal adipose tissue from *Angptl2*$^{-/-}$ and wild-type mice (n = 11–12 per group).

(G) Correlation between F4/80 mRNA expression and epididymal adipose tissue weight in *Angptl2*$^{-/-}$ mice and wild-type mice (n = 11–12 per group). Correlation coefficient (R) and probability (P) values are shown.

(H) Immunohistochemistry of adipose tissue using the macrophage marker MAC2 and adipocyte marker perillipin. Representative photographs and quantitative comparisons of MAC2-positive cells (n = 6 per group) are shown. Scale bar, 100 μm.

(I and J) Glucose (I) and insulin (J) tolerance tests in *Angptl2*$^{-/-}$ mice and wild-type mice (n = 5 and n = 10 per group, respectively).

(K) Insulin signaling in the liver and skeletal muscle of *Angptl2*$^{-/-}$ (KO) and wild-type (WT) mice. Representative western blots and quantitative data for the total and phosphorylated forms of insulin receptor β subunit (IRβ) and Akt are shown (n = 4 per group).

(L) Glucose infusion rate (GIR), glucose disposal rate, endogenous glucose production (EGP) during the basal and clamped states, and percent change in EGP between the states in *Angptl2*$^{-/-}$ (KO) and wild-type (WT) mice (n = 5–7 per group). Data are mean ± SEM, *p < 0.05 and **p < 0.01 compared with controls.

littermates as controls. There was no difference of weight gain between aP2-Angptl2 mice and control wild-type mice fed a normal chow diet (Figure 6A). However, immunohistochemistry using Mac2 revealed accumulation of macrophages in crown-like structures within the adipose tissue of aP2-Angptl2 mice, whereas fewer Mac2-positive cells were observed in wild-type mice (Figure 6B). RT-PCR analysis revealed that inflammatory cytokines (IL-6, TNF-α, and IL-1β) and general (CD68) and inflammatory (CCR2) macrophage markers were increased in the adipose tissue of aP2-Angptl2 mice, while adiponectin and leptin were unchanged (Figure 6C). Lectin staining showed an increase of adherent leukocytes in vessels within the adipose tissue of aP2-Angptl2 mice, while few leukocytes were detected in the vessels of wild-type mice (Figure 6D). There was no

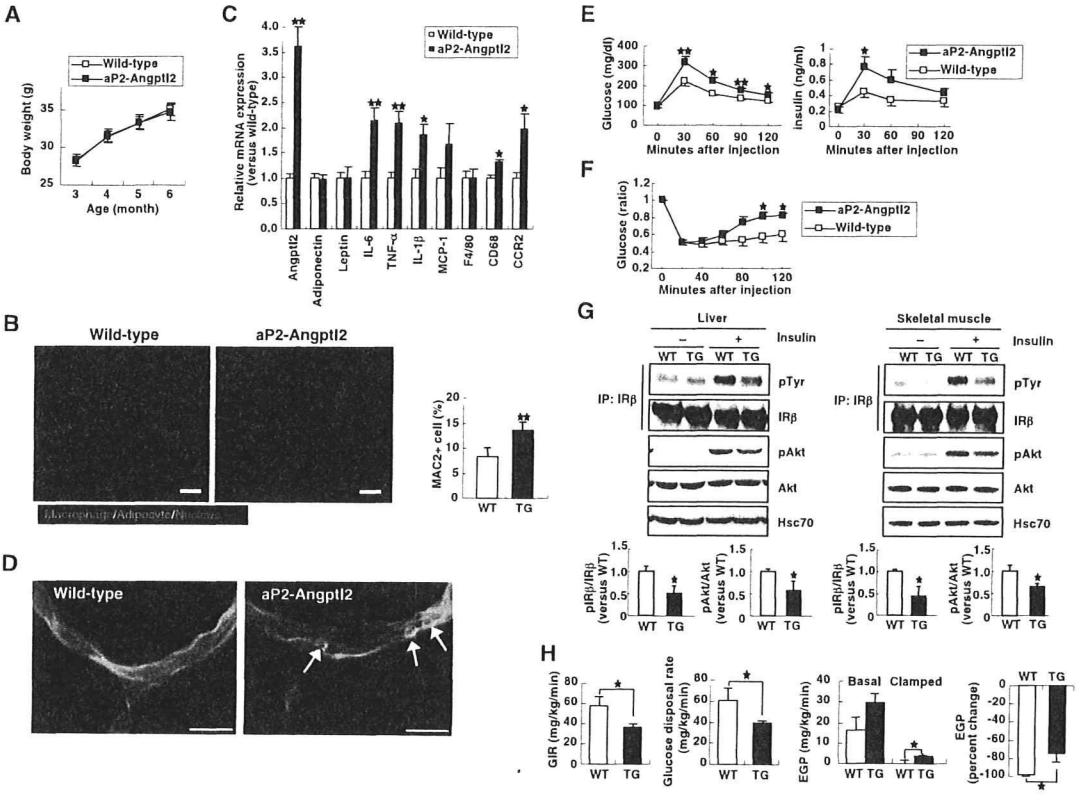

Figure 6. Angptl2 in Adipose Tissue Induces Local Inflammation and Systemic Insulin Resistance

Analyses of aP2-Angptl2 and wild-type mice at 16 weeks of age (B–H).

(A) Body weight of aP2-Angptl2 and wild-type mice (n = 14–16 per group) at the indicated ages (months).

(B) Immunohistochemistry of adipose tissue using the macrophage marker MAC2 and adipocyte marker perillipin. Representative photograghs and quantitative comparison of MAC2-positive cells are shown (n = 6 per group). Scale bar, 50 μm.

(C) Quantitative RT-PCR of mRNAs encoding adipocytokines and macrophage markers in epididymal adipose tissue from aP2-Angptl2 mice and wild-type mice (n = 6 per group).

(D) Blood vessels in epidydimal adipose tissue from aP2-Angptl2 and wild-type mice. Arrows indicate adherent leukocytes on the walls of enlarged vessels in aP2-Angptl2 mice. Scale bar, 25 μm.

(E and F) Glucose (E) and insulin (F) tolerance tests in aP2-Angptl2 mice and wild-type mice (n = 10–12 per group).

(G) Insulin signaling in the liver and skeletal muscle of aP2-Angptl2 (TG) and wild-type (WT) mice. Representative western blots and quantitative data for the total and phosphorylated forms of insulin receptor β subunit (IRβ) and Akt are shown (n = 4 per group).

(H) Glucose infusion rate (GIR), glucose disposal rate, endogenous glucose production (EGP) during the basal and clamped states, and percent change in EGP between the states in aP2-Angptl2 (TG) and wild-type (WT) mice (n = 7 per group). Data are mean ± SEM, $^{*}p < 0.05$ and $^{**}p < 0.01$ compared with controls.

difference of blood vessel density between aP2-Angptl2 mice and control mice (Figure S12C). aP2-Angptl2 mice showed glucose intolerance and insulin resistance in the GTT and ITT, respectively (Figures 6E and 6F). Insulin signaling was diminished in both liver and skeletal muscle of aP2-Angptl2 mice compared with wild-type mice (Figure 6G). The hyperinsulinemic-euglycemic clamp tests also revealed insulin resistance in both skeletal muscle and liver of aP2-Angptl2 mice, since the glucose infusion rate, whole-body glucose disposal rate, and percent change of endogenous glucose production between basal and clamp states were reduced in aP2-Angptl2 mice compared with wild-type mice, while hepatic glucose production during the clamp period was increased in aP2-Angptl2 mice compared with control mice (Figure 6H). These results indicated the presence of insulin resistance in both the skeletal muscle and liver of nonobese aP2-Angptl2 mice.

DISCUSSION

We demonstrated that Angptl2, a member of the Angptl family, is a key mediator of chronic adipose tissue inflammation and obesity-related systemic insulin resistance.

Here we showed that Angptl2 is an adipocyte-derived inflammatory mediator, with increased expression at both the mRNA and protein levels in obesity. Hypoxia and ER stress, which are enhanced in obese adipose tissue (Hosogai et al., 2007; Nishimura et al., 2008; Schenk et al., 2008; Ye, 2009), both increased Angptl2 expression or secretion in adipocytes. Various changes of the microenvironment observed in the adipose tissue of obese animals, such as inflammation and hypoxia, could also promote ER stress (Schenk et al., 2008). Therefore, Angptl2 production by adipocyte should be increased by hypoxia and ER stress in obesity.

It is noteworthy that the circulating Angptl2 level was positively correlated with obesity-related metabolic changes. The difference of circulating Angptl2 protein levels between Angptl2 Tg mice and wild-type mice was only 1.5-fold, but tissue Angptl2 levels showed a 3- to 5-fold difference (data not shown). Therefore, the modest difference of circulating Angptl2 levels in humans may reflect a larger alteration of adipose tissue Angptl2 expression, which could promote inflammation of adipose tissue, resulting in systemic insulin resistance. We also do not exclude the possibility that there is a direct inhibitory effect of circulating Angptl2 on insulin sensitivity in other peripheral tissues, such as skeletal muscle or the liver, because glucose clamp studies and western blotting analysis of insulin signaling revealed that both skeletal muscle and liver were target organs for Angptl2-related insulin resistance in mice. Other Angptl family molecules function in an endocrine manner to regulate lipids, glucose, and energy metabolism (Hato et al., 2008; Oike et al., 2005a, 2005b), so further studies are needed to clarify whether Angptl2 might also act in an endocrine manner.

Angptl2 contains an N-terminal coiled-coil domain and a C-terminal fibrinogen-like domain. The coiled-coil domain is required for oligomerization, which is necessary for its maximum activity, while the fibrinogen-like domain shares high homology with the analogous domain of fibrinogen. Fibrinogen acts as a ligand of the receptors for integrins such as $\alpha v\beta 3$, $\alpha 5\beta 1$, and $\alpha M\beta 2$ (Herrick et al., 1999; Mosesson, 2005), which are heterodimeric transmembrane glycoproteins that mediate cell-extracellular matrix and cell-cell adhesion (Hynes, 2002). Angptl3 was reported to promote angiogenesis through integrin $\alpha v\beta 3$ (Camenisch et al., 2002). In this study, we found that Angptl2 acted on endothelial cells through integrin $\alpha 5\beta 1$ and influenced monocytes/macrophages through integrins $\alpha 4$ or $\beta 2$. Several reports have indicated that integrin $\alpha 5\beta 1$ signaling activates Rac1 in endothelial cells (Dormond et al., 2001; Mettouchi et al., 2001), in agreement with our finding that Angptl2 promotes Rac1 activation in endothelial cells. We also found that Angptl2 induced the chemotaxis of endothelial cells by in vitro time-lapse imaging analysis and an in vivo mouse cornea neovascularization assay. In contrast, constitutive overexpression of Angptl2 in mouse skin or adipose tissue induced pathological vascular inflammation but did not increase vascularization or ameliorate hypoxia in the adipose tissue of mice with dietary obesity (Figure S12D). The cornea is an avascular tissue and thus is isolated from circulating soluble bioactive mediators, whereas various angiogenesis-related factors exist in highly vascular tissues such as the skin and adipose tissue. Taken together, these findings indicate that Angptl2 may function differently in different tissues, but it promotes vascular inflammation rather than angiogenesis, at least in adipose tissue that develops in obese mice.

Potentially relevant to these findings, we observed that Angptl2 stimulated the nuclear translocation of NF-κB and degradation of IκB in cultured vascular endothelial cells, findings consistent with a previous report that integrin $\alpha 5\beta 1$ signaling activates NF-κB-dependent expression of genes that are important for inflammation (Klein et al., 2002). There have been several other reports that Rac1 activates NF-κB (Perona et al., 1997; Sulciner et al., 1996), which is also consistent with our findings. An important aspect of inflammation is the recruitment of immune cells to affected tissues (Luster et al., 2005). This process requires adhesion of the immune cells to endothelial cells, allowing extravasation into the interstitium, followed by adhesion of immune cells to the extracellular matrix that enables migration toward the site of inflammation. In this regard, Angptl2 not only activated NF-κB in endothelial cells, which could induce expression of adhesion molecules (such as ICAM, VCAM, and selectin) and thus facilitate adhesion of immune cells to endothelial cells, but also promoted the migration of monocytes. Immune cells express integrins $\alpha 4$ or $\beta 2$, as well as $\alpha 5\beta 1$, which mediate cell adhesion, migration, activation, and production of proinflammatory cytokines through activation of NF-κB (Hynes, 2002; Rose et al., 2007; Roman et al., 2004; Graves and Roman, 1996), suggesting that Angptl2 may activate monocytes via such integrins. It remains to be clarified whether only Angptl2 among the Angptl family shows a stimulatory effect on adipose tissue inflammation, because some other members of this family bind to integrins (Camenisch et al., 2002), and Angptl4 is also abundantly expressed in adipose tissue. The skin tissue of K14-Angptl4 mice showed no inflammatory changes (Ito et al., 2003), unlike that of K14-Angptl2 mice. Moreover, there was no correlation between the serum Angptl4 concentration and Angptl2-related metabolic factors. These findings suggest that the effects of Angptl4 on endothelial cells and/or immune cells are different from those of Angptl2.

In this study, we demonstrated that Angptl2 deletion not only ameliorated inflammation in adipose tissue but also improved systemic insulin resistance in mice with dietary obesity, although it did not completely normalize their insulin sensitivity to the level seen in mice fed a normal chow diet (Figure S11I). The restoration of insulin sensitivity related to Angptl2 deletion may be attributable to the difference of body fat accumulation between the two genotypes. Since adipose tissue volume was not correlated with macrophage infiltration in *Angptl2*$^{-/-}$ mice, some mechanism other than the difference of adiposity may also have contributed to reducing adipose tissue inflammation in *Angptl2*$^{-/-}$ mice. Actually, constitutive Angptl2 overexpression in adipose tissue induced both local inflammation and systemic insulin resistance in nonobese mice. Since adipose tissue inflammation can be a cause of systemic insulin resistance via the secretion of several inflammatory factors (Apovian et al., 2008; Neels and Olefsky, 2006; Schenk et al., 2008), it is suggested that Angptl2 probably influenced systemic insulin sensitivity by exacerbating adipose tissue inflammation (Figure S13).

Although a reduction of adipose tissue inflammation could well be the main reason for improvement of insulin sensitivity in *Angptl2*$^{-/-}$ mice, some other possible mechanisms remain. Adiponectin can potentially increase insulin sensitivity, and the adiponectin level is usually decreased in obesity (Kadowaki and Yamauchi, 2005). However, there was no difference of circulating adiponecin levels between *Angptl2*$^{-/-}$ and control mice (Figure S11H). On the other hand, *Angptl2*$^{-/-}$ mice had a reduced triglyceride content in both skeletal muscle and liver, which could improve insulin sensitivity in these two organs (Schenk et al., 2008).

Angptl2$^{-/-}$ mice showed reduced body fat and tissue triglyceride accumulation when fed a high-fat diet, although there was no obvious difference of daily food intake and energy expenditure estimated from the O_2 consumption rate. Interestingly, the respiratory quotient of *Angptl2*$^{-/-}$ mice was significantly lower

than that of wild-type mice, suggesting that *Angptl2*$^{-/-}$ mice were more likely to use lipids than carbohydrates for oxidation to create energy. There was also a trend of increased expression of lipid oxidation genes in the skeletal muscle of *Angptl2*$^{-/-}$ mice and increased UCP1 expression in brown adipose tissue (Figures S11D and S11F), which may account for the lower respiratory quotient, decreased triglyceride content of skeletal muscle, and decrease of whole-body fat in *Angptl2*$^{-/-}$ mice. On the other hand, the hepatic expression of lipogenic genes (SREBP-1c, FAS, and SCD1) was significantly decreased in *Angptl2*$^{-/-}$ mice (Figure S11G), which explains the decreased triglyceride content in the liver of these mice, although further studies will be needed to clarify the molecular mechanisms involved.

In summary, this study provided evidence that Angptl2 plays a key role in inflammation of adipose tissue via inflammatory vascular remodeling and recruitment of macrophages into adipose tissue. These findings suggest that Angptl2 may be an important part of the mechanism underlying adipose tissue inflammation that is involved in the pathogenesis of systemic insulin resistance related to obesity. The present findings should also lead to new treatment strategies for obesity and related insulin resistance.

EXPERIMENTAL PROCEDURES

Materials and additional methods are available in the Supplemental Experimental Procedures.

Animal Study

All experimental protocols were approved by the Ethics Review Committee for Animal Experimentation of Kumamoto University. Only male mice were used for the experiments. For the metabolic analyses, mice at 8 weeks of age were fed either a normal diet (CE-2; CLEA, Japan) or a high-fat diet (HFD-32; CLEA) for a period of 8 weeks. During the analyses, mice continued to feed on the same diet.

Human Studies

White adipose tissue samples were obtained from the intact adipose tissue surrounding the tumor resected from a patient with pancreatic carcinoma. Samples were fixed in 4% paraformaldehyde for 24 hr and embedded in paraffin. Sections 5 μm thick were cut and stained with an anti-Angptl2 polyclonal antibody (#383). Nuclei were counterstained with hematoxylin. A total of 98 volunteers working at Kumamoto University were enrolled in the study as the healthy group (persons with obesity [body mass index > 30] or diabetes were excluded). Blood samples were collected, and the plasma glucose, insulin, and CRP levels were measured. A total of 89 patients with type 2 diabetes were enrolled as the DM group. Their abdominal fat content was evaluated by magnetic resonance imaging. The HOMA-R index was calculated as the product of fasting plasma insulin (μU/ml) and fasting plasma glucose (mg/dl) divided by 405 (Matthews et al., 1985). The euglycemic-hyperinsulinemic clamp test was carried out according to a protocol described elsewhere (DeFronzo et al., 1979). A total of 109 patients with coronary artery disease (diagnosed by coronary angiography) were enrolled as the CAD group, and blood samples were collected. Twenty-seven obese diabetic men who had not previously received any antidiabetic agents, antihypertensive agents, or lipid-lowering drugs were treated with pioglitazone at a dose of 30 mg/day for 3 months. Before and after treatment, the abdominal fat content was evaluated by CT scanning, and fasting blood samples were collected to measure the levels of glucose, insulin, and CRP. Blood samples were also collected from 935 consecutive volunteers aged 27–84 years, who underwent medical checkups at the Japanese Red Cross Kumamoto Health Care Center. Serum or plasma levels of Angptl2 and Angptl4 were measured by ELISA. This study was approved by the Ethics Committees of Kumamoto University (healthy and CAD groups), Kobe University (DM group), Ryukyu University (pioglitazone study), and the Japanese Red Cross Kumamoto Health Care Center. Written informed consent was obtained from each subject.

SUPPLEMENTAL DATA

Supplemental Data include Supplemental Experimental Procedures, Supplemental References, 13 figures, one table, and four movies and can be found with this article online at http://www.cell.com/cell-metabolism/supplemental/S1550-4131(09)00232-0.

ACKNOWLEDGMENTS

We would like to thank Ms. K. Fukushima, I. Ishimatsu, R. Shindo, Y. Indo, S. Iwaki, and O. Takahashi for experimental assistance; and Drs. S. Fuchigami, K. Yasunaga, N. Yamaji, and A. Sakurai for experimental assistance and helpful discussion. This work was supported by Grants-in-Aid for Scientific Research on Priority Areas (17014078) from the Ministry of Education, Culture, Sports, Science and Technology of Japan; by Grants-in Aid for Scientific Research (B) (21390245) from Japan Society for Promotion of Science; by a grant from the Mochida Memorial Foundation; by a grant from the Takeda Science Foundation; by a grant from the Sumitomo Foundation; by a grant from the Uehara Memorial Foundation; and by a grant from the Cell Science Research Foundation.

Received: February 3, 2009
Revised: June 5, 2009
Accepted: August 10, 2009
Published: September 1, 2009

REFERENCES

Apovian, C.M., Bigornia, S., Mott, M., Meyers, M.R., Ulloor, J., Gagua, M., McDonnell, M., Hess, D., Joseph, L., and Gokce, N. (2008). Adipose macrophage infiltration is associated with insulin resistance and vascular endothelial dysfunction in obese subjects. Arterioscler. Thromb. Vasc. Biol. *28*, 1654–1659.

Bar-Sagi, D., and Hall, A. (2000). Ras and Rho GTPases: a family reunion. Cell *103*, 227–238.

Camenisch, G., Pisabarro, M.T., Sherman, D., Kowalski, J., Nagel, M., Hass, P., Xie, M.H., Gurney, A., Bodary, S., Liang, X.H., et al. (2002). ANGPTL3 stimulates endothelial cell adhesion and migration via integrin alpha v beta 3 and induces blood vessel formation in vivo. J. Biol. Chem. *277*, 17281–17290.

DeFronzo, R.A., Tobin, J.D., and Andres, R. (1979). Glucose clamp technique: a method for quantifying insulin secretion and resistance. Am. J. Physiol. *237*, E214–E223.

Dormond, O., Foletti, A., Paroz, C., and Ruegg, C. (2001). NSAIDs inhibit alpha V beta 3 integrin-mediated and Cdc42/Rac-dependent endothelial-cell spreading, migration and angiogenesis. Nat. Med. *7*, 1041–1047.

Dvorak, H.F., Senger, D.R., Dvorak, A.M., Harvey, V.S., and McDonagh, J. (1985). Regulation of extravascular coagulation by microvascular permeability. Science *227*, 1059–1061.

Eckel, R.H., Grundy, S.M., and Zimmet, P.Z. (2005). The metabolic syndrome. Lancet *365*, 1415–1428.

Friedl, P., and Weigelin, B. (2008). Interstitial leukocyte migration and immune function. Nat. Immunol. *9*, 960–969.

Fryer, B.H., and Field, J. (2005). Rho, Rac, Pak and angiogenesis: old roles and newly identified responsibilities in endothelial cells. Cancer Lett. *229*, 13–23.

Graves, K.L., and Roman, J. (1996). Fibronectin modulates expression of interleukin-1 beta and its receptor antagonist in human mononuclear cells. Am. J. Physiol. *271*, L61–L69.

Hato, T., Tabata, M., and Oike, Y. (2008). The role of angiopoietin-like proteins in angiogenesis and metabolism. Trends Cardiovasc. Med. *18*, 6–14.

Herrick, S., Blanc-Brude, O., Gray, A., and Laurent, G. (1999). Fibrinogen. Int. J. Biochem. Cell Biol. *31*, 741–746.

Hosogai, N., Fukuhara, A., Oshima, K., Miyata, Y., Tanaka, S., Segawa, K., Furukawa, S., Tochino, Y., Komuro, R., Matsuda, M., and Shimomura, I. (2007). Adipose tissue hypoxia in obesity and its impact on adipocytokine dysregulation. Diabetes *56*, 901–911.

Hynes, R.O. (2002). Integrins: bidirectional, allosteric signaling machines. Cell *110*, 673–687.

Ito, Y., Oike, Y., Yasunaga, K., Hamada, K., Miyata, K., Matsumoto, S., Sugano, S., Tanihara, H., Masuho, Y., and Suda, T. (2003). Inhibition of angiogenesis and vascular leakiness by angiopoietin-related protein 4. Cancer Res. *63*, 6651–6657.

Jackson, J.R., Seed, M.P., Kircher, C.H., Willoughby, D.A., and Winkler, J.D. (1997). The codependence of angiogenesis and chronic inflammation. FASEB J. *11*, 457–465.

Kadowaki, T., and Yamauchi, T. (2005). Adiponectin and adiponectin receptors. Endocr. Rev. *26*, 439–451.

Kanda, H., Tateya, S., Tamori, Y., Kotani, K., Hiasa, K., Kitazawa, R., Kitazawa, S., Miyachi, H., Maeda, S., Egashira, K., and Kasuga, M. (2006). MCP-1 contributes to macrophage infiltration into adipose tissue, insulin resistance, and hepatic steatosis in obesity. J. Clin. Invest. *116*, 1494–1505.

Kim, I., Moon, S.O., Koh, K.N., Kim, H., Uhm, C.S., Kwak, H.J., Kim, N.G., and Koh, G.Y. (1999). Molecular cloning, expression, and characterization of angiopoietin-related protein. angiopoietin-related protein induces endothelial cell sprouting. J. Biol. Chem. *274*, 26523–26528.

Klein, S., de Fougerolles, A.R., Blaikie, P., Khan, L., Pepe, A., Green, C.D., Koteliansky, V., and Giancotti, F.G. (2002). Alpha 5 beta 1 integrin activates an NF-kappa B-dependent program of gene expression important for angiogenesis and inflammation. Mol. Cell. Biol. *22*, 5912–5922.

Kubota, Y., Oike, Y., Satoh, S., Tabata, Y., Niikura, Y., Morisada, T., Akao, M., Urano, T., Ito, Y., Miyamoto, T., et al. (2005a). Cooperative interaction of Angiopoietin-like proteins 1 and 2 in zebrafish vascular development. Proc. Natl. Acad. Sci. USA *102*, 13502–13507.

Luster, A.D., Alon, R., and von Andrian, U.H. (2005). Immune cell migration in inflammation: present and future therapeutic targets. Nat. Immunol. *6*, 1182–1190.

Matthews, D.R., Hosker, J.P., Rudenski, A.S., Naylor, B.A., Treacher, D.F., and Turner, R.C. (1985). Homeostasis model assessment: insulin resistance and beta-cell function from fasting plasma glucose and insulin concentrations in man. Diabetologia *28*, 412–419.

McDonald, D.M. (1994). Endothelial gaps and permeability of venules in rat tracheas exposed to inflammatory stimuli. Am. J. Physiol. *266*, L61–L83.

Mettouchi, A., Klein, S., Guo, W., Lopez-Lago, M., Lemichez, E., Westwick, J.K., and Giancotti, F.G. (2001). Integrin-specific activation of Rac controls progression through the G(1) phase of the cell cycle. Mol. Cell *8*, 115–127.

Mokdad, A.H., Ford, E.S., Bowman, B.A., Dietz, W.H., Vinicor, F., Bales, V.S., and Marks, J.S. (2003). Prevalence of obesity, diabetes, and obesity-related health risk factors, 2001. JAMA *289*, 76–79.

Mosesson, M.W. (2005). Fibrinogen and fibrin structure and functions. J. Thromb. Haemost. *3*, 1894–1904.

Neels, J.G., and Olefsky, J.M. (2006). Inflamed fat: what starts the fire? J. Clin. Invest. *116*, 33–35.

Nishimura, S., Manabe, I., Nagasaki, M., Seo, K., Yamashita, H., Hosoya, Y., Ohsugi, M., Tobe, K., Kadowaki, T., Nagai, R., and Sugiura, S. (2008). In vivo imaging in mice reveals local cell dynamics and inflammation in obese adipose tissue. J. Clin. Invest. *118*, 710–721.

Oike, Y., Yasunaga, K., and Suda, T. (2004). Angiopoietin-related/angiopoietin-like proteins regulate angiogenesis. Int. J. Hematol. *80*, 21–28.

Oike, Y., Akao, M., Kubota, Y., and Suda, T. (2005a). Angiopoietin-like proteins: potential new targets for metabolic syndrome therapy. Trends Mol. Med. *11*, 473–479.

Oike, Y., Akao, M., Yasunaga, K., Yamauchi, T., Morisada, T., Ito, Y., Urano, T., Kimura, Y., Kubota, Y., Maekawa, H., et al. (2005b). Angiopoietin-related growth factor antagonizes obesity and insulin resistance. Nat. Med. *11*, 400–408.

Perona, R., Montaner, S., Saniger, L., Sanchez-Perez, I., Bravo, R., and Lacal, J.C. (1997). Activation of the nuclear factor-kappaB by Rho, CDC42, and Rac-1 proteins. Genes Dev. *11*, 463–475.

Roman, J., Ritzenthaler, J.D., Boles, B., Lois, M., and Roser-Page, S. (2004). Lipopolysaccharide induces expression of fibronectin alpha 5 beta 1-integrin receptors in human monocytic cells in a protein kinase C-dependent fashion. Am. J. Physiol. Lung Cell. Mol. Physiol. *287*, L239–L249.

Rose, D.M., Alon, R., and Ginsberg, M.H. (2007). Integrin modulation and signaling in leukocyte adhesion and migration. Immunol. Rev. *218*, 126–134.

Schenk, S., Saberi, M., and Olefsky, J.M. (2008). Insulin sensitivity: modulation by nutrients and inflammation. J. Clin. Invest. *118*, 2992–3002.

Sulciner, D.J., Irani, K., Yu, Z.X., Ferrans, V.J., Goldschmidt-Clermont, P., and Finkel, T. (1996). rac1 regulates a cytokine-stimulated, redox-dependent pathway necessary for NF-kappaB activation. Mol. Cell. Biol. *16*, 7115–7121.

Weisberg, S.P., Hunter, D., Huber, R., Lemieux, J., Slaymaker, S., Vaddi, K., Charo, I., Leibel, R.L., and Ferrante, A.W., Jr. (2006). CCR2 modulates inflammatory and metabolic effects of high-fat feeding. J. Clin. Invest. *116*, 115–124.

Ye, J. (2009). Emerging role of adipose tissue hypoxia in obesity and insulin resistance. Int. J. Obes. *33*, 54–66.

Am J Physiol Endocrinol Metab 297: E1291–E1303, 2009.
First published September 15, 2009; doi:10.1152/ajpendo.00293.2009.

Different impacts of saturated and unsaturated free fatty acids on COX-2 expression in C_2C_{12} myotubes

Akito Kadotani,[1,2] Yo Tsuchiya,[3] Hiroyasu Hatakeyama,[3] Hideki Katagiri,[2] and Makoto Kanzaki[1,3,4]

[1]*Center for Research Strategy and Support;* [2]*Division of Advanced Therapeutics for Metabolic Diseases, Center for Translational and Advanced Animal Research;* [3]*Graduate School of Biomedical Engineering, Tohoku University, Sendai and* [4]*Japan Science and Technology Agency, Core Research for Evolutionary Science and Technology, Tokyo, Japan*

Submitted 7 May 2009; accepted in final form 7 September 2009

Kadotani A, Tsuchiya Y, Hatakeyama H, Katagiri H, Kanzaki M. Different impacts of saturated and unsaturated free fatty acids on COX-2 expression in C_2C_{12} myotubes. *Am J Physiol Endocrinol Metab* 297: E1291–E1303, 2009. First published September 15, 2009; doi:10.1152/ajpendo.00293.2009.—In skeletal muscle, saturated free fatty acids (FFAs) act as proinflammatory stimuli, and cyclooxygenase-2 (COX-2) is a pro/anti-inflammatory enzyme induced at sites of inflammation, which contributes to prostaglandin production. However, little is known about the regulation of COX-2 expression and its responses to FFAs in skeletal muscle. Herein, we examined the effects of saturated and unsaturated FFAs, including a recently identified lipokine (lipid hormone derived from adipocytes), palmitoleate, on COX-2 expression in C_2C_{12} myotubes as a skeletal muscle model. Exposure of myotubes to saturated FFAs [palmitate (16:0) and stearate (18:0)], but not to unsaturated FFAs [palmitoleate (16:1), oleate (18:1), and linoleate (18:2)], led to a slow-onset induction of COX-2 expression and subsequent prostaglandin E_2 production via mechanisms involving the p38 MAPK and NF-κB but not the PKCθ signaling cascades. Pharmacological modulation of mitochondrial oxidative function failed to interfere with COX-2 expression, suggesting the mitochondrial overload/excessive β-oxidation contribution to this event to be minimal. On the contrary, unsaturated FFAs appeared to effectively antagonize palmitate-induced COX-2 expression with markedly different potencies (linoleate > oleate > palmitoleate), being highly associated with the suppressive profile of each unsaturated FFA toward palmitate-evoked intracellular signals, including p38, JNK, ERK1/2 MAPKs, and PKCθ, as well as IκB degradation. In addition, our data suggest little involvement of PPAR in the protective actions of unsaturated FFAs against palmitate-induced COX-2 expression. No direct contribution of the increased COX-2 activity in generating palmitate-induced insulin resistance was detected, at least in terms of insulin-responsive Akt phosphorylation and GLUT4 translocation. Taken together, our data provide a novel insight into the molecular mechanisms responsible for the FFA-induced COX-2 expression in skeletal muscle and raise the possibility that, in skeletal myocytes, COX-2 and its product prostaglandins may play an important role in the complex inflammation responses caused by elevated FFAs, for example, in the diabetic state.

cyclooxygenase-2; inflammation; signal transduction; glucose transporter 4; insulin resistance

ACCUMULATING EVIDENCE DEMONSTRATES A POTENTIAL LINK between metabolic disorders (such as type 2 diabetes, obesity, and atherosclerosis) and chronic low-grade inflammation, characterized by abnormal cytokine production and activation of a network of inflammatory signaling pathways in insulin target tissues such as fat, liver, and skeletal muscle (26, 54). Although these inflammatory responses have been recognized as being triggered by lipid-laden adipose tissue under obese conditions (20), recent studies demonstrate that skeletal muscle also secretes a number of proinflammatory cytokines, [e.g., interleukin (IL)-6, tumor necrosis factor (TNF)α] in response to various stimuli including exercise (39) and elevated levels of free fatty acids (FFAs) (29, 30). Indeed, it has been reported that exposure of skeletal muscle cells to saturated FFAs, especially palmitate (C16:0), induces insulin resistance and increased secretion of these proinflammatory cytokines; however, oleate (C18:1), an unsaturated FFA, does not have such deleterious effects, instead antagonizing these palmitate-induced responses (9, 10, 29, 30). Intriguingly, palmitoleate (C16:1), another unsaturated FFA derived from adipose tissue and thereby termed a lipokine (lipid hormone), has been suggested to directly regulate skeletal muscle metabolism and insulin responsiveness (5). However, details of the mechanisms underlying the actions of saturated and unsaturated FFAs and the potential role of palmitoleate in pro/anti-inflammatory responses of skeletal muscle remain unclear.

Several lines of evidence have also indicated the involvement of inducible cyclooxygenase (COX)-2 and its proinflammatory prostaglandin (PG) products in metabolic disorders, including type 2 diabetes (28, 32). On the other hand, some COX-2 metabolites, such as cyclopentenone PGs, have been shown to exert anti-inflammatory actions (18, 45). In contrast to constitutively expressed COX-1, COX-2 is promptly induced by various proinflammatory stimuli (17). COX-2 can convert arachidonate (20:4) released by cytosolic phospholipase A2 from membrane phospholipids into PGH_2, which is further metabolized into biologically active end products such as PGE_2 by multiple specific enzymes in a cell type-restricted fashion (17). In the context of metabolic disorders, elevated PGE_2 synthesized via macrophage COX-2 contributes to plaque rupture in atherosclerosis (4). Also, COX-2 upregulations in the pancreas, mesangial tissue, and peripheral tissue are associated with chronic diabetic pancreatitis (35), diabetic nephropathy (33), and diabetic peripheral neuropathy (46), respectively. In addition, COX-2 (+/−) heterozygote mice are reportedly obese, although the underlying mechanism remains unclear (15). In skeletal muscle, physical exercise has been shown to induce COX-2 expression (31, 52), which appeared to play a role in the regulation of muscle functions, including muscle differentiation, healing, and regeneration (2, 25). However, no study has investigated the effects of saturated and unsaturated FFAs on COX-2 expression in skeletal muscle cells. In addition, detailed signaling mechanisms directly involved in the induction of COX-2 expression in skeletal muscle are poorly understood.

Address for reprint requests and other correspondence: M. Kanzaki, Graduate School of Biomedical Engineering, Tohoku University, 2-1 Seiryo-machi, Aoba-ku, Sendai 980-8575, Japan (e-mail: kanzaki@bme.tohoku.ac.jp).

The detrimental effects of saturated FFAs such as palmitoleate (C16:0) in skeletal muscle cells have been attributed to abnormal accumulation of palmitoyl-CoA, diacylglycerol, and/or ceramide, which in turn leads to deleterious activation of various serine/threonine kinases such as PKCθ (19, 30, 49). PKCθ, a novel PKC isoform expressed abundantly in skeletal muscle cells, has a unique ability to activate transcriptional factor NF-κB, and the PKCθ-NF-κB signaling cascade has been shown to play an important role in the production of IL-6 and TNFα in skeletal muscle cells (9, 29, 30, 53). Intriguingly, the antagonizing action of oleate (18:1) against palmitate-induced responses has been at least partially explained by a mechanism involving suppression of the PKCθ/NF-κB signaling cascades by oleate (9, 29, 30). On the other hand, saturated FFAs also reportedly activate members of the MAPK family, including ERK1/2, p38, and JNK (10, 11, 51), although their possible involvement in proinflammatory responses in skeletal muscle cells is poorly understood. Furthermore, a detailed analysis of the different impacts of saturated and unsaturated FFAs on these intracellular signaling cascades in skeletal muscle cells has yet to be reported.

In this study, we evaluated the effects of saturated and unsaturated FFAs on proinflammatory COX-2 expression and the involved intracellular signals, such as p38, JNK, ERK1/2 MAPKs, PKCθ, and NF-κB, in C_2C_{12} skeletal muscle cells. We also examined the protective action of unsaturated FFAs against the palmitate-evoked events. Our findings are the first to shed light on the regulation of FFA-induced COX-2 expression and intracellular signals in skeletal muscle.

MATERIALS AND METHODS

Materials. The Western blot detection kit (West super femto detection reagents) and Immobilon-P were purchased from Pierce Biotechnology (Rockford, IL) and Millipore (Bedford, MA), respectively. Dulbecco's modified Eagle's medium (DMEM), penicillin-streptomycin, and trypsin-EDTA were purchased from Sigma Chemical (St. Louis, MO). Cell culture equipment was obtained from BD Biosciences (San Jose, CA). Calf Serum (CS) and fetal bovine serum (FBS) were purchased from BioWest (Nuaille, France). FFA free-bovine serum albumin (BSA) was purchased from Wako Pure Chemical Industries (Osaka, Japan). Anti-COX-2, anti-p38, anti-phospho-p38 (Thr^{180}/Tyr^{182}), anti-phospho-PKCθ (Thr^{538}), anti-JNK, anti-phospho-JNK (Thr^{183}/Tyr^{185}), anti-ERK1/2, anti-phospho-ERK1/2 (Thr^{202}/Tyr^{204}), anti-IκBα, and anti-phospho-activating transcription factor-2 (ATF-2) ($Thr^{69/71}$) antibodies were purchased from Cell Signaling Technology (Danvers, MA). Anti-β-actin antibody was purchased from Sigma. The ELISA kit for PGE_2 was purchased from R & D Systems (Minneapolis, MN). Fatty acids, pyrrolidine dithiocarbamate (PDTC), SB-203580, rottlerin, etomoxir, thenoyltrifluoroacetone (TTFA), and carbonyl cyanide *m*-chlorophenylhydrazone (CCCP) were purchased from Sigma. Wy-14643, GW-501516, and 20:4 were purchased from Cayman Chemicals (Ann Arbor, MI), Alexis Biochemicals (Lausen, Switzerland), and MP Biomedicals (Solon, OH), respectively. Other chemicals were purchased from Sigma or Wako.

Cell culture. Mouse skeletal muscle cell lines, C_2C_{12} myoblasts, were maintained in DMEM supplemented with 10% FBS, 30 μg/ml penicillin, and 100 μg/ml streptomycin (growth medium) at 37°C under a 5% CO_2 atmosphere. For biochemical study, the cells were grown on six-well plates (BD Biosciences) at a density of 3×10^4 cells/well in 3 ml of growth medium. Three days after plating, cells had reached ~80–90% confluence (*day 0*). Differentiation was then induced by replacing the growth medium with DMEM (4.5 g/l glucose) supplemented with 2% CS, 1 nM insulin, 30 μg/ml penicillin, and 100 μg/ml streptomycin (differentiation medium) (40). The differentiation medium was changed every 24 h, and the differentiated cells (on *days 4* and *5*) were used for subsequent experiments. For immunofluorescence analysis, cells were grown on 22-mm glass coverslips (C022221; Matsunami, Osaka, Japan) in six-well plates. FFA-containing media were prepared by preincubation of FFA with DMEM supplemented with 2% FFA-free BSA, as described previously (30). Inhibitors were prepared in dimethylsulfoxide and then added to media at 0.1% (vol/vol).

Quantitative real-time PCR. Total RNA was prepared using the TRIzol reagent (Invitrogen, Carlsbad, CA), following the manufacturer's instructions. Quantitative real-time PCR analysis was performed using the Light Cycler instrument and SYBR Green detection kit according to the manufacturer's instructions (Roche Diagnostics, Indianapolis, IN). PCR primers for COX-2 were 5′-AGA TCA TAA GCG AGG ACC TG-3′ and 5′-TAC ACC TCT CCA CCA ATG AC-3′.

Western blot analysis. Cell lysates were prepared using lysis buffer [50 mM Tris·HCl, pH 7.4, 150 mM NaCl, 1 mM EDTA, 1% NP-40, 1 μg/ml pepstatin, 5 μg/ml leupeptin, 1 mM phenylmethylsulfonyl fluoride, 6,500 IU/ml aprotinin, phosphatase inhibitor cocktail-1 (Sigma)], and the protein concentrations of cell lysates were then measured using the BCA protein assay kit (Pierce Biotechnology). Proteins (20 μg) were subjected to 10% SDS-polyacrylamide gel electrophoresis and then transferred to a PVDF membrane (Immobilon-P), and the membranes were then blocked for 2 h at room temperature with 5% nonfat dry milk in Tris-buffered saline containing 0.1% Tween-20. The membranes were next immunoblotted with primary antibodies at dilutions of 1:500 to 1:1,000. Specific total or phospho-proteins were visualized after subsequent incubation with a 1:10,000 dilution of anti-mouse or rabbit IgG conjugated to horseradish peroxidase and the SuperSignal Chemiluminescence detection procedure (Pierce Biotechnology). Three independent experiments were performed for each condition.

ELISA for PGE_2. PGE_2 levels in media were evaluated using the PGE_2 Parameter Assay Kit (R & D Systems).

Immunofluorescence analysis. C_2C_{12} myotubes were cultured on coverslips placed on six-well plates. After differentiation, the cells were treated with or without 1 mM palmitate for 16 h. Then the cells were fixed with 2% paraformaldehyde in PBS (−) and permeabilized using 0.4% Triton X-100 in PBS (−), followed by immunocytochemistry using anti-COX-2 antibody (Cell Signaling Technology), and anti-rabbit IgG antibody conjugated with Alexa 594 (Invitrogen). F-actin was visualized by Oregon Green 488 phalloidin (Invitrogen). Images were monitored and analyzed using Olympus Fluoview FV1000 confocal microscopy and the associated application program ASW Ver1.3 (Olympus, Tokyo, Japan).

Anti c-myc antibody uptake assay. Glucose transporter 4 (GLUT4) translocation was analyzed as described previously (41). Briefly, C_2C_{12} myotubes expressing myc-GLUT4-enhanced cyan fluorescent protein (ECFP) were serum-starved, washed three times with Krebs-Ringer-Pi-HEPES buffer, and then placed in a CO_2 incubator with 2 ml of Krebs-Ringer-Pi-HEPES buffer. After 10 min of incubation, 4 μg/ml anti-c-myc antibody was added to the buffer, and the cells were stimulated with or without 100 nM insulin for 30 min. After incubation for 30 min with the anti-myc antibody, the cells were placed on ice to stop the reaction and washed five times with PBS. The cells were harvested using 1× Laemmli's buffer and subjected to Western blot analysis using anti-mouse IgG antibody and anti-c-myc antibody.

Statistical analysis. Data are expressed as means ± SE. Statistical significance was determined by ANOVA followed by the Bonferroni-Dunn post hoc test using StatView software (SAS Institute). Differences were considered significant when P values were <0.05.

RESULTS

Saturated, but not unsaturated, FFAs induce COX-2 expression in C_2C_{12} myotubes. Utilizing mouse skeletal muscle line C_2C_{12} cells, we examined the effects of FFAs on the mRNA expression of COX-2 (Fig. 1*A*). Treatment with palmitate (C16:0) or stearate (C18:0) for 16 h dramatically induced COX-2 mRNA expression in a dose-dependent manner in

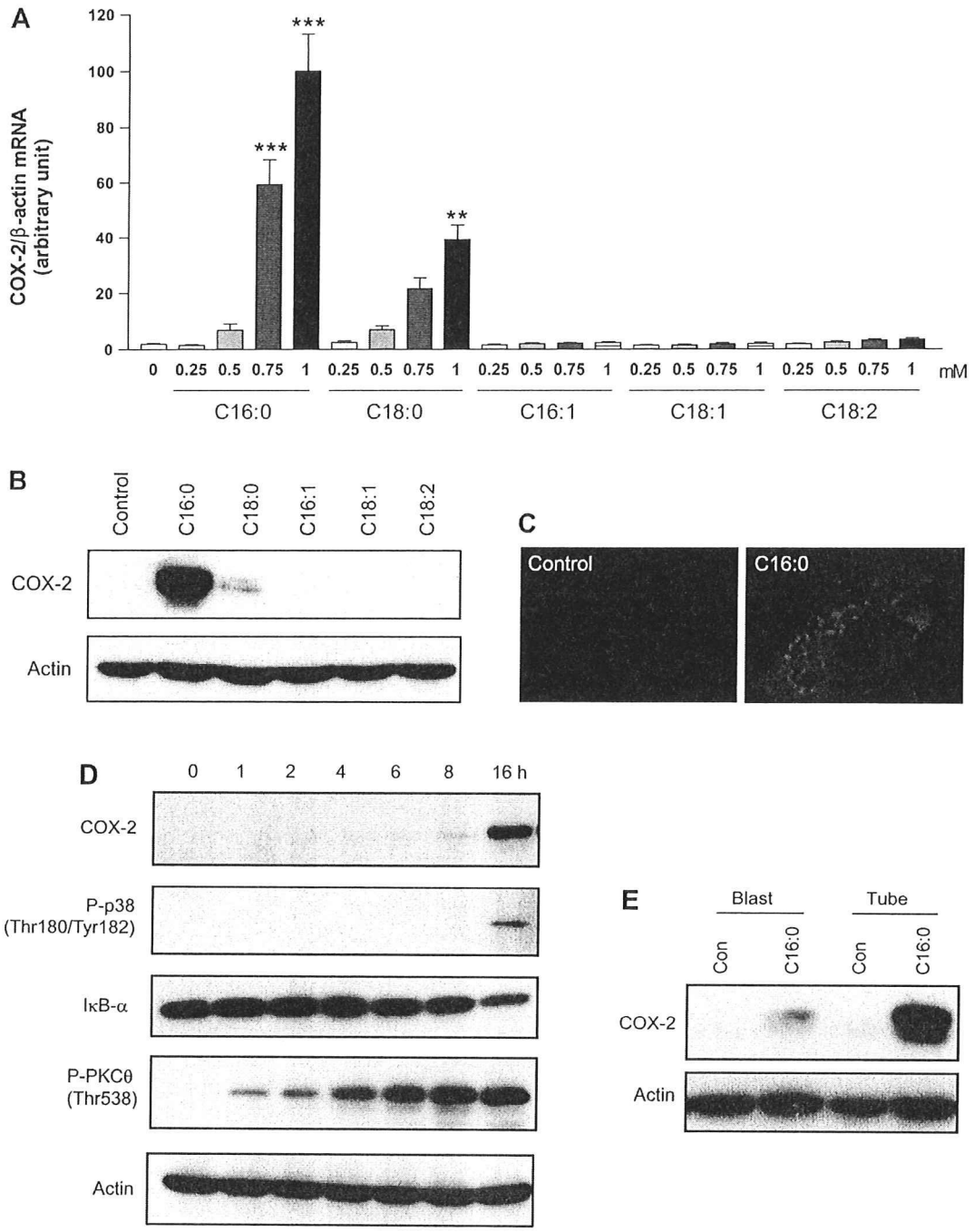

Fig. 1. Effects of saturated and unsaturated fatty acids on cyclooxygenase-2 (COX-2) expression in C_2C_{12} myotubes. *A*: C_2C_{12} myotubes were treated with free fatty acids (FFAs) for 16 h, and total RNA was then prepared. mRNA levels of COX-2 and β-actin (control) were quantified by real-time PCR. FFAs were expressed as follows: C16:0, palmitate; C18:0, stearate; C16:1, palmitoleate; C18:1, oleate; C18:2, linoleate. Data are expressed as means ± SE of 3 independent experiments (**$P <$ 0.005, ***$P < 0.0005$ vs. untreated control). *B*: C_2C_{12} myotubes were treated with 1 mM FFA for 16 h, and the cell lysates were then subjected to Western blot analysis. *C*: C_2C_{12} myotubes were treated with (C16:0) or without (control) 1 mM palmitate for 16 h, and immunofluorescence analysis was then performed (red, COX-2; blue, F-actin). *D*: C_2C_{12} myotubes were treated with 1 mM palmitate for 1–16 h, and the cell lysates were then subjected to Western blot analysis. *E*: C_2C_{12} myoblasts (blast) or myotubes (tube) were treated with (C16:0) or without [control (Con)] 1 mM palmitate for 16 h, and the cell lysates were then subjected to Western blot analysis.

C_2C_{12} myotubes, and the effective dose was >0.75 mM. Expression of COX-1 mRNA was not increased by palmitate treatment (data not shown). In contrast to saturated FFAs, unsaturated FFAs [palmitoleate (C16:1), oleate (C18:1), and linoleate (C18:2)] had no effects on the COX-2 mRNA level. Consistent with these mRNA data, Western blot analysis demonstrated that only saturated FFAs, especially palmitate (C16:0), strongly induce COX-2 protein (Fig. 1*B*), and this was

further confirmed by immunofluorescent staining using anti-COX-2 antibody (Fig. 1*C*).

Time course experiments revealed COX-2 protein to be detectable after 16 h of palmitate treatment (Fig. 1*D*), apparently accompanied by enhanced phosphorylation of p38 (Thr^{180}/Tyr^{182}) and slight degradation of IκBα (Fig. 1*D*). On the contrary, slight PKCθ phosphorylation (Thr^{538}) was detected after as little as 1 h of treatment and was further augmented thereafter, reaching a plateau after 6 h of stimulation. Differentiated C_2C_{12} myotubes were highly responsive to palmitate, in terms of this COX-2 expression, whereas myoblasts were far less responsive.

To further characterize the palmitate-induced COX-2 expression and the intracellular signal(s) possibly involved, we conducted detailed dose-response analyses of the effects of palmitate on the amount of COX-2 protein, the phosphorylation status of p38 and PKCθ, and the amount of IκB protein in C_2C_{12} myotubes (Fig. 2, *A–E*). Consistent with the mRNA data, 16-h treatment with pathophysiologically relevant concentrations of palmitate (>0.75 mM) increased cellular COX-2 protein contents (Fig. 2, *A* and *B*), resulting in increased accumulation of PGE_2, a bioactive product of COX-2, in conditioned media (Fig. 2*F*). The palmitate-induced phosphorylations of p38 (Fig. 2, *A* and *C*) and PKCθ (Fig. 2, *A* and *D*) were both sensitively detected even when relatively low concentrations of palmitate were applied and peaked at 0.75 mM of palmitate. The degradation of IκB as assessed by the total amount of IκB was also observed at palmitate concentrations >0.75 mM (Fig. 2*E*). Since physiological levels of circulating FFAs are reportedly between 0.3 and 0.4 mM, rising to 0.6–0.8 mM in obese or type 2 diabetes patients (1, 30), these data indicate that the saturated FFA-induced COX-2 expression observed herein may be a phenomenon occurring only at hyperphysiological FFA levels, approximating pathophysiological conditions.

Taken together, these results indicate that saturated FFAs, but not unsaturated FFAs, induce COX-2 expression in C_2C_{12} myotubes. Our data also raise the possibility that the p38- and/or PKCθ-NF-κB pathway may be involved in palmitate-induced COX-2 expression and PGE_2 production in C_2C_{12} myotubes.

p38 and NF-κB are involved in palmitate-induced COX-2 expression in C_2C_{12} myotubes. To define the involvement of p38 and PKCθ as well as that of NF-κB in palmitate-induced COX-2 expression, C_2C_{12} myotubes were incubated with 1 mM palmitate for 16 h in the presence or absence of selective pharmacological inhibitors for NF-κB (PDTC), p38 (SB-203580), or PKCθ (rottlerin) (Figs. 3 and 4). PDTC, an NF-κB inhibitor, significantly reduced the COX-2 protein expression induced by palmitate in a dose-dependent manner, and this expression was almost entirely suppressed by a high dose of PDTC (Fig. 3, *A* and *B*). Similarly, SB-203580, a p38 inhibitor, dose-dependently blocked palmitate-induced COX-2 expression (Fig. 3, *C* and *D*), whereas phosphorylations of PKCθ and p38 as well as IκB degradation were unchanged (Fig. 3*C*). As expected, phosphorylation of ATF-2, a substrate of p38, was also significantly suppressed in the presence of SB-203580 (Fig. 3*E*), indicating that SB-203580 did indeed inhibit p38 enzymatic activity under these experimental conditions. On the contrary, rottlerin (an inhibitor of novel PKCs) failed to affect the COX-2 protein expression induced by palmitate (Fig. 4, *A* and *B*), although PKCθ phosphorylation was dose-dependently decreased by rottlerin (Fig. 4, *A* and *C*). The phosphorylation and total amount of p38 were, as expected, unaffected by rottlerin (Fig. 4*A*). Although phosphorylation of JNK, another stress-activated MAPK, was increased by palmitate treatment (Fig. 6*A*), inhibition of JNK by SP600125 failed to interfere with COX-2 expression (data not shown). Overall, these results indicate that p38 and NF-κB are involved in regulation of the COX-2 expression induced by palmitate, but our experimental evidence revealed no contribution of PKCθ to this COX-2 expression despite PKCθ phosphorylation being strongly augmented by palmitate treatment.

Mitochondrial fatty acid oxidation may not be involved in COX-2 expression. Mitochondrial overload and incomplete fatty acid oxidation may contribute to insulin resistance (36) as well as to inflammatory responses in skeletal muscle. Thus, we next investigated the possibility that fatty acid oxidation is involved in COX-2 expression by using pharmacological inhibitors for enzymes related to fatty acid oxidation (Fig. 5). However, etomoxir (carnitine palmitoyltransferase I inhibitor), TTFA (electron transport complex II inhibitor), and CCCP (an uncoupler of oxidative phosphorylation) all failed to exert any inhibitory effect on palmitate-induced COX-2 expression (Fig. 5*A*).

We also examined the effect of 2-bromopalmitate (2-BP) on COX-2 expression, since 2-BP is a nonmetabolizable palmitate analog (8). One mM of 2-BP had no ability to induce COX-2 expression (Fig. 5*B*). Taken together, these results indicate that palmitate metabolism is apparently required for COX-2 expression, whereas fatty acid oxidation in mitochondria is not directly involved in this event in C_2C_{12} myotubes.

Unsaturated fatty acids reverse palmitate-induced COX-2 expression. Physiologically, saturated and unsaturated FFAs are both present in blood and cells, and previous studies demonstrated that oleate (C18:1) reverses palmitate-induced insulin resistance and IL-6 production (9). Recently, palmitoleate (C16:1) was proposed to serve as a lipokine that communicates with both the liver and skeletal muscles and regulates systemic metabolic homeostasis (5). Therefore, we evaluated the impacts of unsaturated fatty acids on palmitate-induced COX-2 protein expression as well as on the related intracellular signals activated by palmitate (Fig. 6). Unsaturated FFAs displayed remarkable dose-dependent inhibitory effects on all of the palmitate-induced events analyzed (Fig. 6). Importantly, potencies against palmitate-induced responses differed significantly among these unsaturated fatty acids, although their patterns were similar (linoleate > oleate > palmitoleate), and sufficient concentrations of each unsaturated fatty acid completely abolished palmitate-induced COX-2 protein expression (Fig. 6, *A* and *B*) as well as the related PGE_2 production (Fig. 6*J*).

Unexpectedly, despite clear dose-responsive suppression of COX-2 protein expression by these unsaturated FFAs, the phosphorylation status of p38 did not correspond well to this change. This phenomenon was exemplified by 30 μM linoleate producing a slight but significant enhancement of the palmitate-induced phosphorylation of p38 instead of inhibiting it. Moreover, these unsaturated FFAs failed to dampen p38 phosphorylation status to the basal level (Fig. 6*C*), whereas they clearly abolished the palmitate-induced phosphorylation of ATF-2 (Fig. 6*D*) as well as that of JNK (Fig. 6*F*), another upstream kinase responsible for ATF-2 phosphorylation (21). Although the molecular mechanism(s) underlying the bell-shaped dose-response profile of p38 phosphorylation at Thr^{180}/Tyr^{182} under mixed FFA conditions remains to be clarified, the observation that unsaturated FFAs

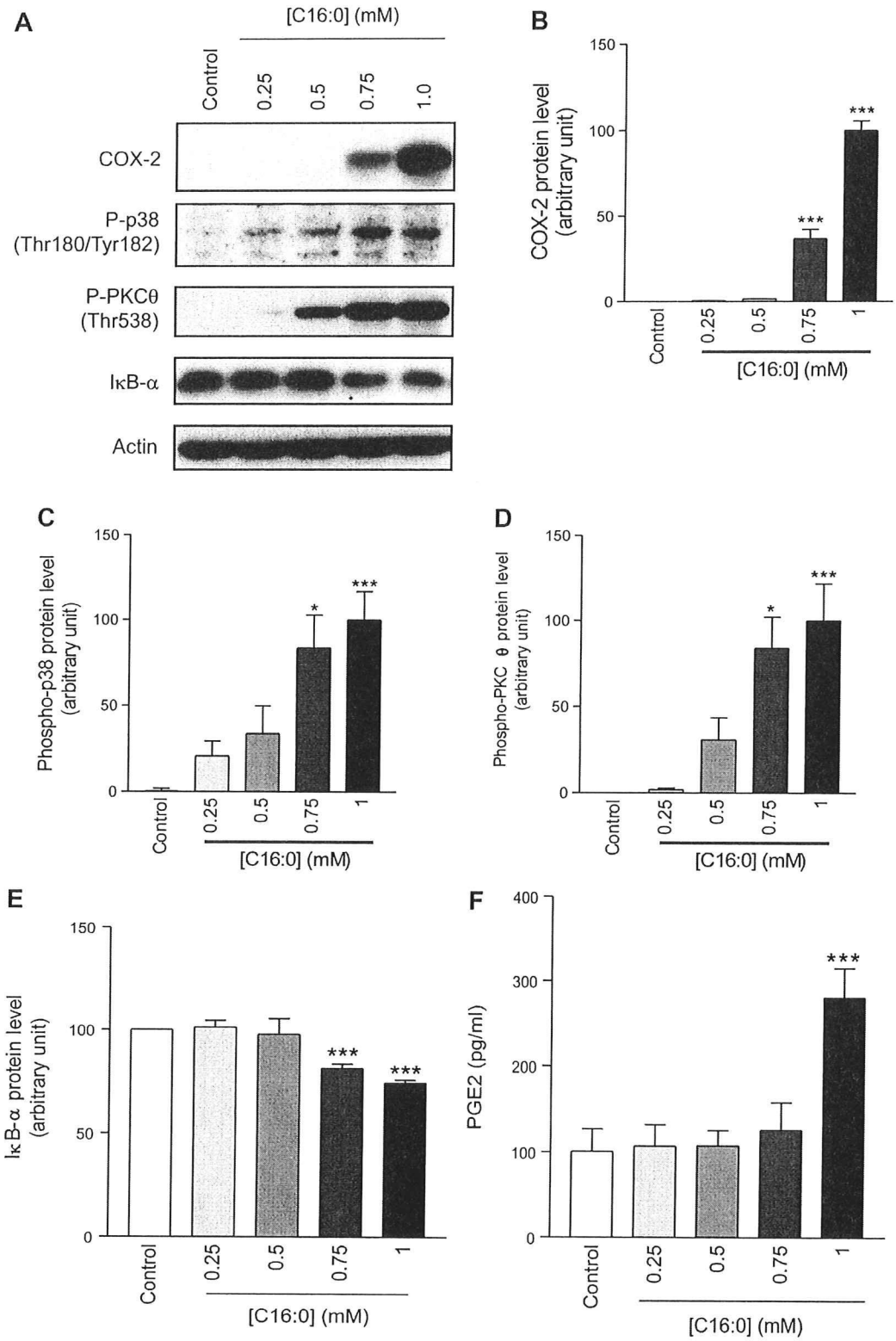

Fig. 2. Effects of palmitate on signaling pathways via p38 or PKC and prostaglandin E_2 (PGE_2) production. *A–E*: C_2C_{12} myotubes were treated with 0.25–1 mM palmitate for 16 h, and the cell lysates were then subjected to Western blot analysis (*A*). Specific bands of COX-2 (*B*), phospho-p38 (*C*), phospho-PKCθ (*D*), and IκB-α (*E*) were quantified using a densitometer. Data are expressed as means ± SE of 3 independent experiments (*$P < 0.005$, ***$P < 0.0005$ vs. control). *F*: C_2C_{12} myotubes were treated with 0.25–1 mM palmitate for 16 h, and the media were then collected. PGE_2 levels in the media were measured by ELISA. Data are expressed as means ± SE of 6 independent experiments (***$P < 0.005$ vs. control).

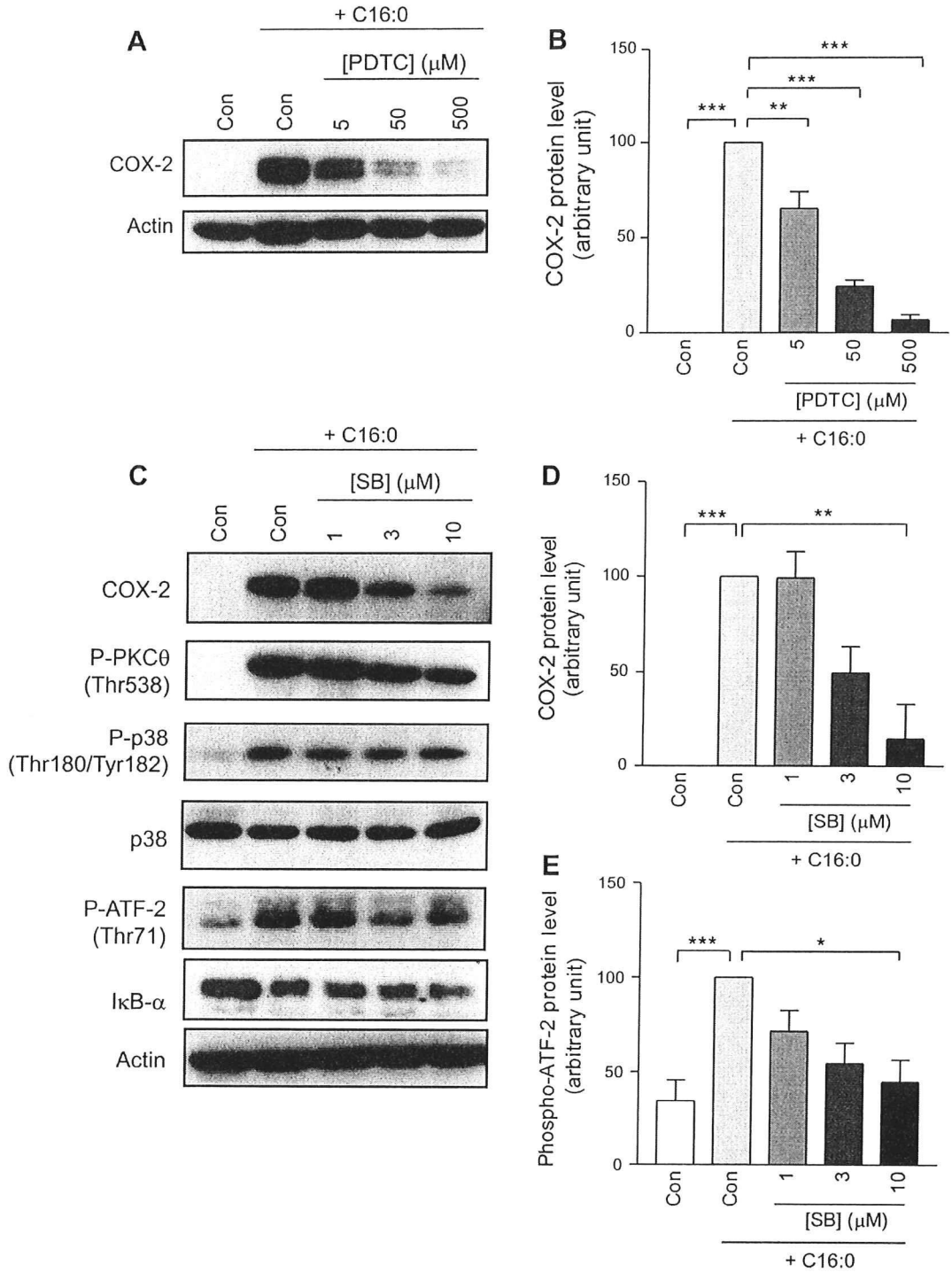

Fig. 3. Effects of pharmacological inhibition of NF-κB and p38 on palmitate-induced COX-2 expression. *A* and *C*: C_2C_{12} myotubes were treated with or without 1 mM palmitate (C16:0) in the presence of several concentrations of pyrrolidine dithiocarbamate (PDTC; NF-κB inhibitor) or SB-203580 (SB; p38 inhibitor) for 16 h, and the cell lysates were then subjected to Western blot analysis. *B*, *D*, and *E*: specific bands in the Western blots were quantified using a densitometer. Data are expressed as means ± SE of 3 independent experiments (*$P < 0.05$, **$P < 0.005$, ***$P < 0.0005$ vs. control).

abolish palmitate-induced ATF-2 phosphorylation (Fig. 6*D*) strongly suggests that signaling cascades reaching ATF-2 are effectively hampered by administering unsaturated FFAs, although they have markedly different potencies.

Neither PPARα nor PPARβ/δ is involved in the protective actions of unsaturated FFAs against palmitate-induced COX-2 expression and p38 MAPK activation. To explore possible mechanisms underlying the protective effects of unsaturated

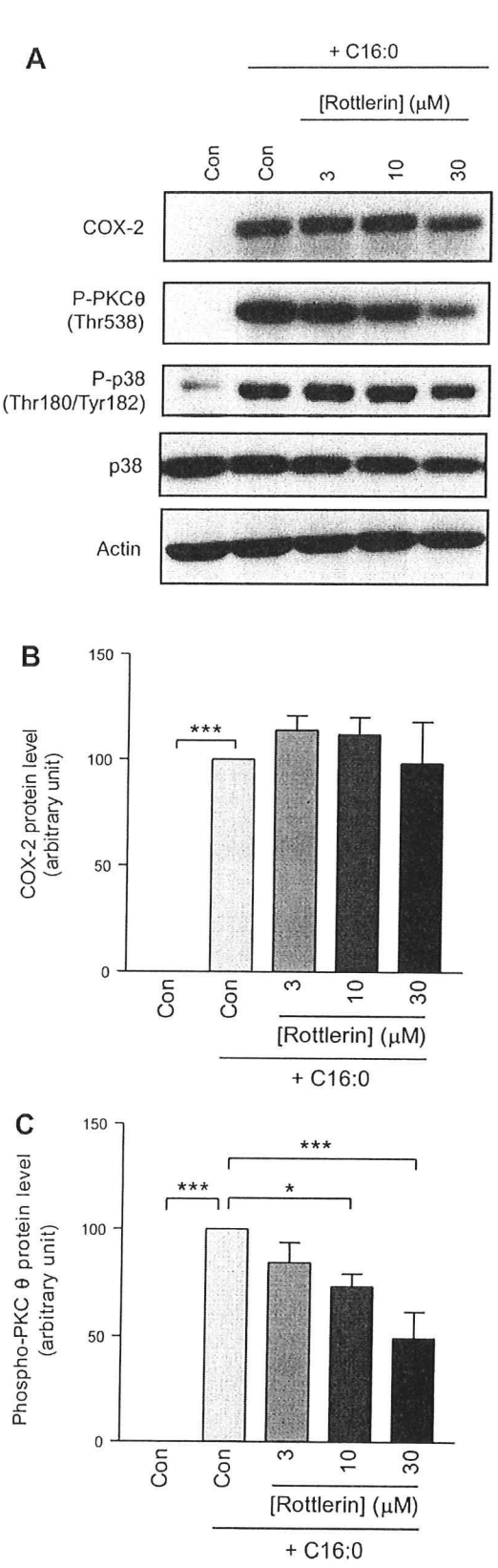

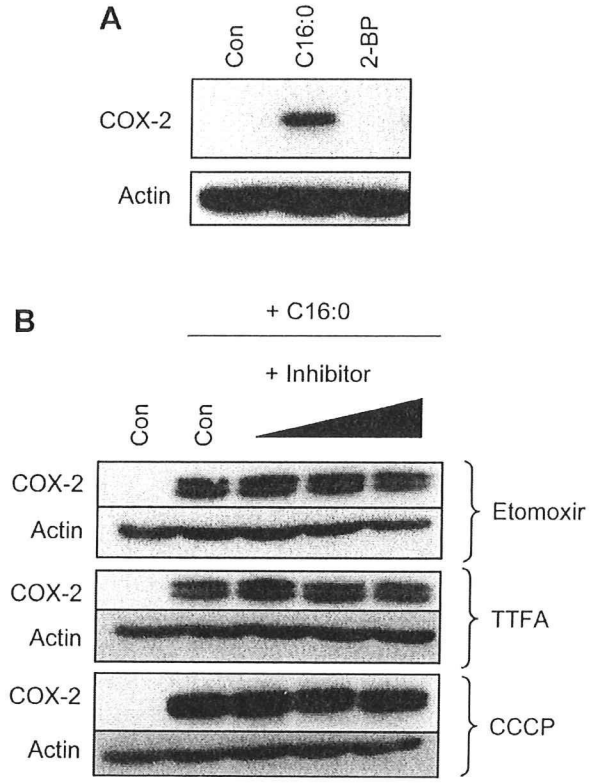

Fig. 5. Effects of inhibition of fatty acid oxidation or 2-bromopalmitate (2-BP) on palmitate-induced COX-2 expression. *A*: C_2C_{12} myotubes were treated with or without 1 mM palmitate (C16:0) in the presence of several concentrations of etomoxir (200, 500, and 1,000 μM; carnitine palmitoyl transferase I inhibitor), thenoyltrifluoroacetone (TTFA; 10, 30, and 100 μM; electron transport complex II inhibitor), or CCCP (0.5, 3, and 10 μM; uncoupler) for 16 h. The cell lysates were then subjected to Western blot analysis. *B*: C_2C_{12} myotubes were treated with 1 mM palmitate (C16:0) alone or in combination with 1 mM 2-BP (a nonmetabolizable analog of palmitate) for 16 h. The cell lysates were subjected to Western blot analysis.

FFAs on the palmitate-induced events in C_2C_{12} myotubes, we examined the effects of several agonists of peroxisome proliferator-activated receptor (PPAR) on palmitate-induced events, since unsaturated FFAs have been shown to serve as potent ligands for these PPARs (16). The palmitate-induced events were reversed completely by arachidonate (20:4; also known as an endogenous PPAR pan-agonist) (16) but not by Wy-14643 (PPARα agonist) or GW-501516 (PPARβ/δ agonist) (34, 42), indicating that PPARs may not be involved in the protective actions of unsaturated FFAs against palmitate-induced events.

Effect of pharmacological inhibition of COX-2 on palmitate-induced insulin resistance in C_2C_{12} myotubes. Finally, we examined the possible involvement of COX-2 and its metabolites in the generation of insulin resistance in C_2C_{12}

Fig. 4. Effects of pharmacological inhibition of PKCθ on palmitate-induced COX-2 expression. *A*: C_2C_{12} myotubes were treated with or without 1 mM palmitate (C16:0) in the presence of 3–30 μM rottlerin (a novel PKC-specific inhibitor) for 16 h, and the cell lysates were then subjected to Western blot analysis. *B* and *C*: specific bands in the Western blots were quantified using a densitometer. Data are expressed as means ± SE of 3 independent experiments ($^*P < 0.05$, $^{***}P < 0.0005$ vs. control).

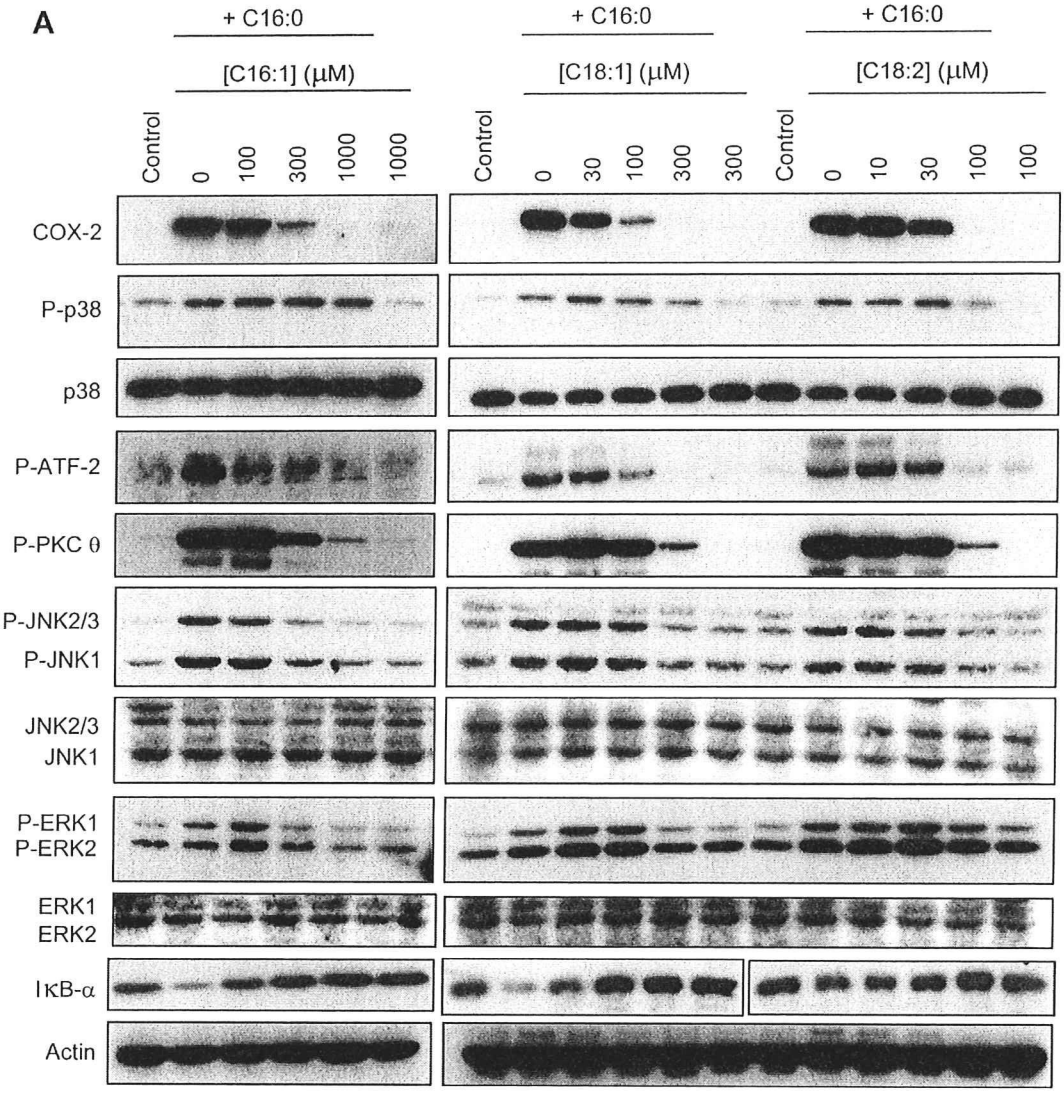

Fig. 6. Effects of unsaturated fatty acids (USFA) on palmitate-induced COX-2 expression, its signaling pathways, and PGE_2 production. *A–I*: C_2C_{12} myotubes were treated with 1 mM palmitate (C16:0) alone or in combination with palmitoleate (C16:1), oleate (C18:1), or linoleate (C18:2) for 16 h, and the cell lysates were then subjected to Western blot analysis (*A*). Specific bands in the Western blots were quantified using a densitometer. Data are expressed as means ± SE of 3 independent experiments ($^*P < 0.05$, $^{**}P < 0.005$, $^{***}P < 0.0005$ vs. control; *B–I*). *J*: PGE_2 levels in the media were measured by ELISA. Data are expressed as means ± SE of 4 independent experiments ($^{**}P < 0.005$, $^{***}P < 0.0005$ vs. control).

myotubes. We employed a myc-GLUT4 translocation assay using anti-myc antibody, as reported previously (41). Insulin-induced Akt phosphorylation was also examined to monitor insulin receptor signals. As reported previously (6, 50), palmitate (1 mM) treatment obviously suppressed insulin-induced Akt (Ser^{473}) phosphorylation, which was not restored by NS-398, a COX-2-selective inhibitor (Fig. 8*A*). As expected, insulin-responsive GLUT4 translocation was also impaired by this palmitate treatment, with impaired insulin responsiveness being partially attributable to the increased GLUT4 translocation even in the basal state (Fig. 8*B*). Consistent with the Akt phosphorylation data, NS-398 failed to restore the impaired insulin-induced GLUT4 translocation in palmitate-treated C_2C_{12} myotubes (Fig. 8, *B* and *C*).

DISCUSSION

Palmitate-induced COX-2 expression requires the activities of p38 MAPK and NF-κB but not that of PKCθ. In the present study, we observed phosphorylation of PKCθ (Thr^{538}) by palmitate treatment within 1 h (Fig. 1*D*). However, a relatively longer period (~16 h) was required for COX-2 expression, and pharmacological inhibition of this enzyme by rottlerin failed to inhibit palmitate-induced COX-2 expression (Fig. 4), although the NF-κB activity was apparently required for this event (Fig. 3, *A* and *B*). These results strongly suggest that activation of PKCθ alone was insufficient for rapid induction of COX-2 expression via activation of NF-κB in C_2C_{12} myotubes instead indicating that delayed activation of p38 is additionally required for COX-2 expres-

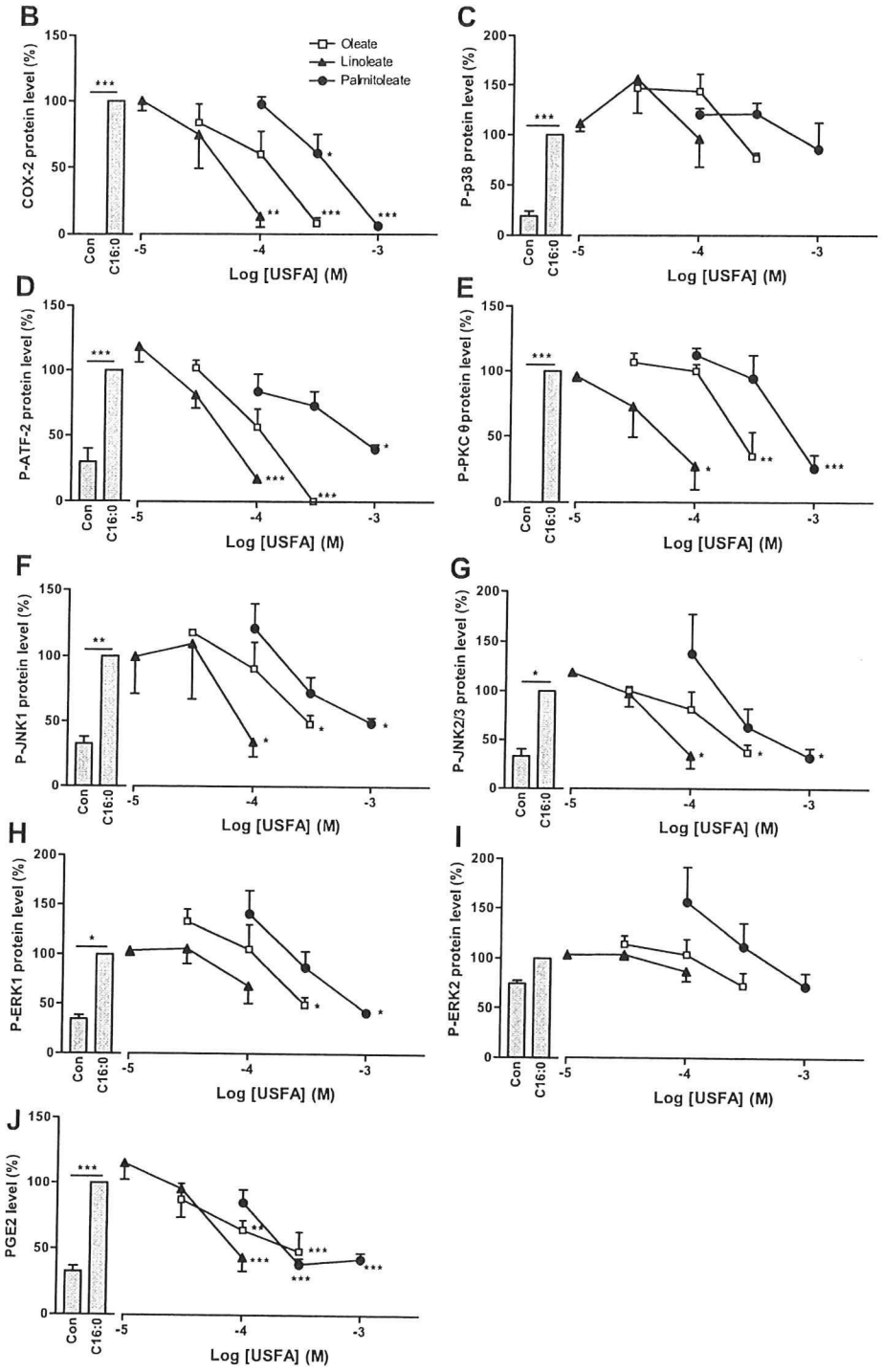

Fig. 6.—*Continued*

sion (Fig. 3, *C–E*). In this regard, a recent study demonstrated that both DNA binding and transcriptional activation of NF-κB began to rise in cultured myotubes after an 8-h incubation with palmitate (24). Moreover, p38 has been shown to directly regulate NF-κB phosphorylation and its nuclear localization in cardiac myocytes (55), and direct involvement of the p38-ATF-2 pathway in the regulation of COX-2 expression has also been reported in other cell types (23, 43). Supporting this notion is our observation that SB-203580 failed to reverse the IκB degradation elicited by palmitate treatment (Fig. 3*C*), suggesting p38 activity to be crucial for COX-2 expression to function independently of

IκB degradation. Taking these observations together, although PKCθ-mediated NF-κB activation via palmitate-induced intracellular lipid accumulation has been implicated in the increased secretion of IL-6 and TNFα (9, 29, 30, 53), our present data provide compelling evidence that p38 MAPK, but not PKCθ, serves as the crucial signaling intermediate for the COX-2 expression in C_2C_{12} skeletal muscle cells. A similar mechanism was also observed for the palmitate-induced suppression of PGC-1α expression in skeletal muscle cells (10, 11).

Mitochondrial overload, ceramide, and Toll-like receptors do not play a crucial role in palmitate-induced COX-2 expression. An interesting observation reported herein is that inhibition of fatty acid oxidation by various reagents that modulate mitochondrial respiration and reactive oxygen species (ROS) generation totally failed to influence palmitate-induced COX-2 expression (Fig. 5), which would appear to contradict a recent report showing that mitochondrial overload with excessive β-oxidation could be a major cause of insulin resistance in skeletal muscle (36). Because 1 mM of a halogenated analog of palmitate, 2-BP (22), has no COX-2-inducible effect, a specific fatty acyl-CoA moiety and/or palmitate metabolism is apparently required for COX-2 expression (Fig. 5). In addition, it has been reported that mitochondria-derived ROS is a key initiator for the phosphorylation of p38 (37). Since we have not examined the effects of supplemental carnitine, which reportedly tends to be deficient in cell cultures and thereby partially obliterates actual mitochondrial performance (36), we cannot as yet exclude the involvement of mitochondrial ROS generation in palmitate-induced COX-2 expression. Elucidation of this possibility requires further experiments.

Although it has been reported that palmitate can activate the proinflammatory pathway via a Toll-like receptor-dependent mechanism(s) (12, 51), we observed no inhibitory effects of blocking antibodies against Toll-like receptor-2/4 on palmitate-induced COX-2 expression (data not shown). We also examined the possible involvement of ceramide in COX-2 expression by utilizing a cell-permeable C2-ceramide (50). However, 100 μM C2-ceramide did not induce COX-2 expression in C_2C_{12} myotubes (data not shown), indicating ceramide itself to be insufficient for reproducing palmitate-induced COX-2 expression, although ceramide accumulation might contribute to this event in conjunction with other palmitate-induced component(s).

Effects of unsaturated FFAs on COX-2 expression and intracellular signals evoked by palmitate treatment. Although a recent report proposed the importance of palmitoleate (16:1) serving as an adipose-derived lipid hormone (lipokine) (5), our findings indicate that palmitoleate, in contrast

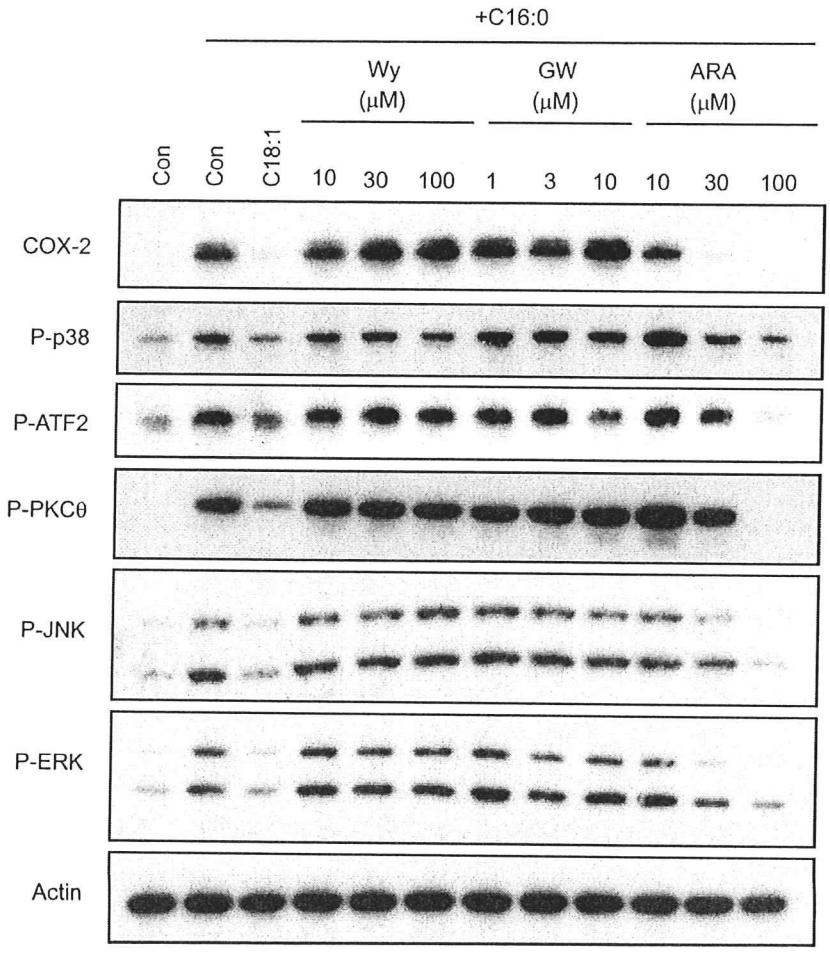

Fig. 7. Effects of Wy-14643 (Wy), GW-50156 (GW), and arachidonate (ARA) on palmitate-induced COX-2 expression and its signaling pathways. C_2C_{12} myotubes were treated with 1 mM palmitate (C16:0) alone or in combination with 300 mM oleate (C18:1) and several concentrations of Wy, GW, or ARA for 16 h. The cell lysates were then subjected to Western blot analysis. Three independent experiments were performed, and representative results were obtained. ATF-2, activating transcription factor-2.